Nuclear Instruments and Methods in Physics Research A 346 (1994) 329–352
North-Holland

NUCLEAR
INSTRUMENTS
& METHODS
IN PHYSICS
RESEARCH
Section A

A large air shower array to search for astrophysical sources emitting γ-rays with energies $\geq 10^{14}$ eV

A. Borione, C.E. Covault, J.W. Cronin, B.E. Fick, K.G. Gibbs, H.A. Krimm, N.C. Mascarenhas, T.A. McKay, D. Müller, B.J. Newport, R.A. Ong, L.J Rosenberg, H. Sanders
Department of Physics and Enrico Fermi Institute University of Chicago, Chicago, IL 60637, USA

M. Catanese, D. Ciampa, K.D. Green, J. Kolodziejczak, J. Matthews, D. Nitz, D. Sinclair, J.C. van der Velde
Department of Physics University of Michigan, Ann Arbor, MI 48109, USA

(Received 4 February 1994)

We describe the technical details and the performance of a large array which detects both the electron and muon components in extensive air showers with energies $\geq 10^{14}$ eV. The array was designed to search for γ-rays from astrophysical sources. The background of cosmic rays is reduced by the selection of muon poor events. The array consists of 1089 scintillation detectors on the surface covering an area of 0.23 km^2 and 1024 scintillation counters of 2.5 m^2 each, buried 3 m below the surface for muon detection. Each of the surface detectors has its own local electronics and local data storage controlled by a microprocessor. The array is located at Dugway, Utah USA (40.2°N, 112.8°W) where the average atmospheric depth is 870 g/cm^2.

1. Introduction

At the 1960 International Cosmic Ray Conference, Cocconi suggested that large airshower arrays could be used to search for very high energy γ-rays from astrophysical objects [1]. In 1983 a seminal paper was published by Samorski and Stamm [2] in which the detection of γ-rays $\sim 10^{15}$ eV from the X-ray binary Cygnus X-3 was reported. These results appeared to be confirmed by Lloyd–Evans et al. [3] and Kifune et al. [4]. These observations, which were made with rather small arrays, stimulated the construction of arrays specifically designed for γ-ray astronomy [5,6]. In general, these arrays are much larger and have thresholds $\leq 10^{14}$ eV. Several reviews of the progress of this field over the past few years can be found elsewhere [7].

In this paper we will give a detailed description of the Chicago Air Shower Array (CASA) and a review of the Michigan Muon Array (MIA). Section 2 begins with an overview of the architecture of CASA followed by a description of its components. Section 3 describes the components of MIA. In Section 4 we describe the calibration of the array and its properties including angular resolution, hadron rejection, and shower size determination. In Section 5 we describe our experience with the operation of the array.

CASA has been described partially in previous publications [8]. The buried muon counters of MIA have also been described [9].

2. The surface array (CASA)

2.1. Overview of the design

We began the design of CASA with the goals of high counting rate, good angular resolution and effective hadron rejection. The latter requirement led us to choose the Dugway site because a large area of buried muon counters were being installed by some of us around the Fly's Eye II fluorescence detector [10] to work in conjunction with the Utah air shower array [6].

The design was optimized for signals from sources like Cygnus X-3, whose integral spectrum was reported to fall as E^{-1}. Since the cosmic ray background spectrum falls as $E^{-1.7}$, the signal-to-background should improve as the energy increases. Using the criteria of minimizing the time to obtain a signal of a given significance while keeping the number of detectors fixed, we found a broad minimum with detector spacings in the range of 10 to 20 m. We chose then a spacing of 15 m and a size such that we would receive ≥ 20 events per day from a source of the reported strength of Cygnus X-3 [2]. With such a design we would observe ~ 200 events from a source with a flux of 10^{-11} cm^{-2} s^{-1} during a single passage overhead. These considerations led to our design of a surface array of 1089 detectors on a grid of 15 m covering an area of 2.3×10^5 m^2. Fig. 1 shows a plan view of the array.

SSDI 0168-9002(94)00221-R

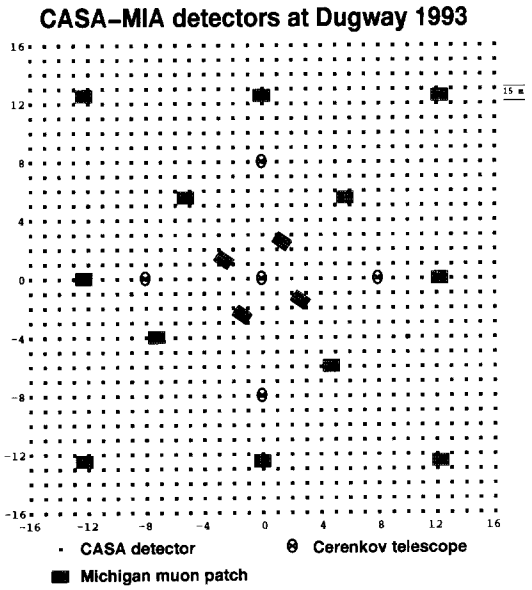

Fig. 1. Plan view of the CASA and MIA arrays. The buried muon counters are collected in patches of 64 individual counters. The five Cherenkov telescopes, built by the University of Utah, are used for resolution measurement and direction calibration. The Fly's Eye II detector which lies in the center of the array is not shown.

While in many respects the design of the surface array is conventional, we considered the normal arrangement, in which each station contains a single scintillation counter with its signal and high-voltage cables running to centralized electronics, to be impractical for such a large number of stations. Instead we chose to place all the electronics locally within each station, which has the advantage that long, high-quality cable runs are not required to preserve the nanosecond timing required for good angular resolution. We placed within each station four scintillation counters and required at least a double coincidence before a detector was recorded as part of a shower. This requirement reduced the effective singles rate of an individual station to $\sim$ 10–20 Hz. Triple coincidences are indicative of the presence of a shower and are used as the basis for triggering the array. Finally, when a coincidence occurs in a given station, a pulse is sent by a twisted pair cable to each of its four nearest neighbors. With this technique, the relative time of arrival of the shower front at each station is determined and the need for a clock synchronized over the entire array is eliminated.

The array operates as follows: If two or more scintillation counters fire within 30 ns the station is said to be *alerted*. If three or more scintillators fire within 30 ns the station is said to be *triggered* as well as alerted. Each triggered station places a standard 5 mA current pulse of 10 μs duration (*trigger request*) on a cable which is connected to a central control. If three or more such quanta of current are detected by the central control, the trigger condition for the whole array is satisfied and a *trigger acknowledge* pulse (−12 V of 2 μs duration) is sent to all stations. At the time of an alert, the station is disabled and eight time-to-digital converters (TDCs) are started by the coincidence pulse. Four of the TDCs are stopped by delayed pulses from the scintillation counters in the station. The other four TDCs are stopped by the coincidence pulses (if present) from the nearest neighbor stations. The time standard for each TDC is a temperature-stabilized local oscillator. The amplitude of each scintillation counter is recorded by charge integrators. These times and amplitudes are stored temporarily as DC voltages. If a trigger acknowledge pulse is received within 10 μs of the alert time, the voltages are digitized and stored in a local memory. Following the digitization the station is reenabled. If no trigger acknowledge is received within 10 μs of the alert time the TDCs and charge integrators are reset and the station is reenabled. Each station is controlled by a microprocessor. The data are stored in one-half of a 3 kByte local memory. Periodically the data storage is switched to the other half of the memory and the data stored in the inactive memory is read out sequentially from each station by an Ethernet system. This arrangement has the advantage of very small dead time, the largest component of which is the 0.5 ms required to digitize the event.

In the following sections we describe the various components of the array. In the design we were guided by the need to operate over a temperature range of −10°C to 50°C, the requirement of no moving parts, and the need for extreme economy. These latter criteria led us to use, as much as possible, materials and electronic components that had broad commercial applications.

2.2. The CASA station

2.2.1. Mechanical and electrical design

Fig. 2 shows the mechanical arrangement of a station. Four scintillation counters are placed in a UV resistant ABS plastic box specially designed for the purpose. The box is stiffened by a wooden cross structure glued to the bottom which defines the cells for the location of the four scintillation counters. A plywood surface is attached to the wooden cross for support of the local electronics and its power supplies. A styrofoam pillar is placed in the center to provide support for the lead converter sheets placed on top of each station. The lead converter sheets initially were painted white which reduced the ambient temperature within the box by about 4°C during the summer months.

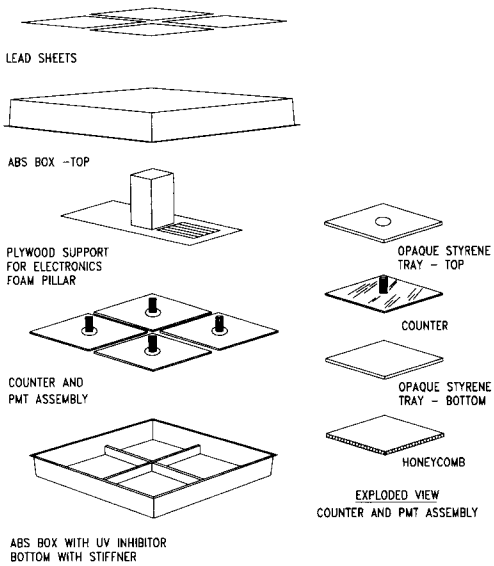

Fig. 2. Exploded view of a CASA station.

The boxes are sealed against water leaks by one inch wide weatherstripping. Initially the top and bottom half of the boxes were held together by plastic rivets but it was found that the weight of the lead sheets was sufficient to secure the joint. After installation in the field cracks developed in the corners of many boxes causing, in some cases, serious water damage. To avoid this we have fitted each box with a weatherproof cover. These covers made of white material have eliminated the need for painting the lead.

The AC powerlines, trigger-request cables and trigger-acknowledge cables are distributed through a central spine running east and west from the central control. Each north-south row of stations is called a rib. The arrangement of the ribs and spine is shown in Fig. 3. The inflow of the trigger request current pulses from each rib on RG-58 cable is transferred to an RG-8 cable on the spine by a repeater. These repeaters detect the trigger current level on the ribs by means of a set of parallel comparator circuits. The pulses are reformed and sent out on the spine trigger cable, preserving the original timing structure of the input pulses. The outgoing trigger acknowledge pulses are carried on RG-58 cable throughout and are transferred to the ribs by a repeater. Two phase power is also distributed along the spine. Single phase 120 V power is tapped off to each rib in a manner to keep the load balanced on each phase. Power is available in each station by means of a standard household receptacle. An extra receptacle is available for a soldering iron or oscilloscope for repairs or troubleshooting. Nearest neighbor stations are connected by two twisted pair cables which transmit the TDC start pulse of a station to its neighbor and vice versa. All these cables are contained within commercial 3.5 cm diameter black polyethylene pipe which is coupled to the sides of the plastic boxes with standard plastic fittings.

2.2.2. Survey of the stations

The positions of the CASA stations were laid out in advance of installation using a laser ranging theodolite. The positions were placed on a nearly perfect 15 m grid, with a few deviations to avoid the removal of trees. The orientation of the grid is such that the x-axis runs east–west and y-axis runs north–south. After installation the position of each station was surveyed along with its height relative to a survey monument. Several survey monuments were used to cover the whole array. A number of stations were surveyed from different monuments to search for systematic errors. The deviations from a perfect grid are characterized by an RMS of 0.035 m. The deviation of the y-axis from true north was checked by the observation of five stars with the theodolite. The y-axis of the array was found to be rotated from true north by $(0.063 \pm 0.01)°$ clockwise. The site slopes from the north-east to the south-west with a total change in height of ~ 10 m.

2.2.3. Scintillation counters

Each scintillation counter is made of a 61 cm $\times$ 61 cm $\times$ 1.27 cm sheet of acrylic scintillator [11]. For purposes of economy the edges of the scintillator remained sawcut. A 5 cm diameter photomultiplier tube was glued in the middle of the plastic with a ~ 0.5 mm thick layer of two component RTV (GE-655) [12]. Experience led us to use a thick flexible joint to avoid broken joints due to the extreme variations in temperature. Two types of PMTs were used in approximately equal numbers, 12-stage Amperex 2212 obtained from a neutrino experiment at Brookhaven National Laboratory, and 10-stage EMI 9256 purchased especially for CASA. The typical high voltage is 1300 V for the 10 stage tubes, and is 1900 V for the 12 stage tubes.

The uniformity of light collection is poor in such a counter design. The amount of light collected is to a

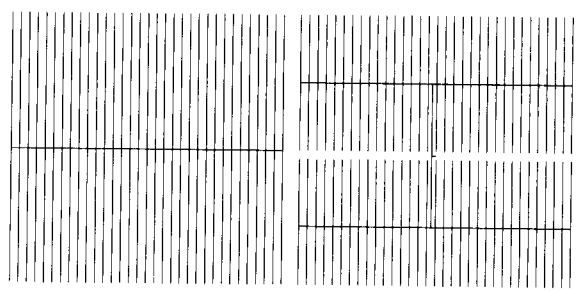

Fig. 3. The layout of the CASA trigger spine and rib system (left) and the dual-spine Ethernet system (right).

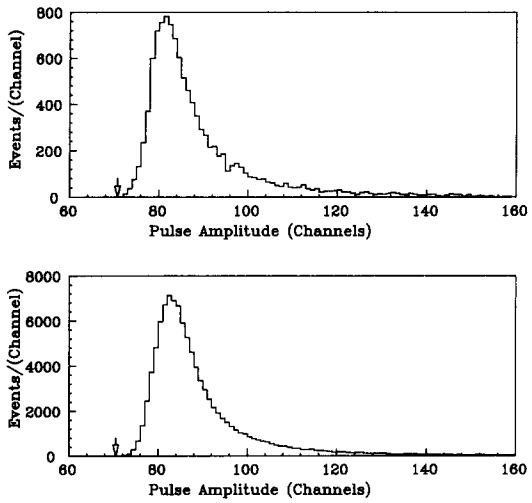

Fig. 4. Above, pulse amplitude distribution for a CASA scintillation counter exposed to vertical muons distributed uniformly over its surface. Below, distribution of pulse amplitudes based on a simulation of the r^{-1} dependence of the light collection. The arrow indicates the position of the pedestal.

good approximation proportional to the distance of the source of light to the center. On average we estimate that about 10 photoelectrons are collected when a minimum ionizing charged particle passes through an extreme corner of the counter. In Fig. 4a we plot the pulse amplitude distribution for one of these counters for uniform illumination with single vertical muons as measured on a test stand. This pulse amplitude distribution can be understood by a simple model of the light collection. When a charged particle crosses the scintillator, the light trapped by total internal reflection spreads radially in all directions. The light aimed toward the photocathode is efficiently collected giving a dependence r^{-1} where r is the distance between the source of the scintillation light and the center of the phototube. Shown in Fig. 4b is the pulse amplitude distribution calculated on the basis of this form of light collection. The calculation assumes that vertically incident minimum ionizing particles are uniformly distributed over the counter. Each counter is ultimately calibrated in-situ with the abundant cosmic rays which trigger the array. A description of this process is given in section 4.2.2.

2.2.4. Electronics

The electronics for each station is mounted on a single six layer circuit board measuring 30 cm × 45 cm. It was designed at the University of Chicago by a collaboration of physicists and engineers at the Enrico Fermi Institute. The design of the station electronics with its many functions represented the greatest intellectual challenge in the construction of CASA.

Each board consumes about 18 watts and uses low power CMOS logic whenever possible. Special switching power supplies were designed for the board [13]. These supplies provide five independent voltages. The supplies were optimized to have maximum efficiency. The total power consumed by each station is 24 watts.

The high voltage for the four PMT's in each station is supplied by a single 12 V to 3000 V DC/DC converter [14] mounted in a separate housing which plugs

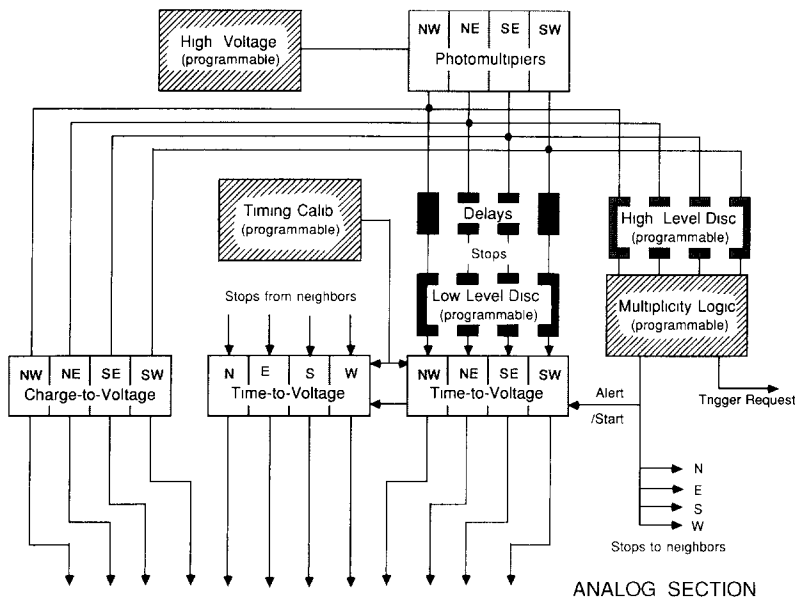

Fig. 5. Schematic diagram of the analog electronics.

into the main board. This makes its replacement easy in the field. The high voltage is regulated by a feedback circuit located on the board. The high voltage level can be set by remote command from the central station. During assembly the four PMT's placed in each station were selected to have approximately the same gain when operated at the same voltage. The EMI tubes were purchased with bases which draw 0.1 mA. The Amperex tubes had bases which draw 0.25 mA and were just within the limit of the power capacity of the converter. The PMT's are operated with their photocathodes at ground potential.

A schematic diagram of the analog section of the electronics is shown in Fig. 5. Each PMT signal enters the board through a short 50 Ω twisted pair cable using an inexpensive 0.1 in. connector [15]. Most connections to the board used this hardware. Fast comparators (Linear Technology LT1016) serve as discriminators. The input signal from each PMT is fed into a high level and a low level discriminator. The high level is set to ~ 24 mV and the low level to one third of that value. The PMT voltage is set so that the high level discriminator corresponds to ~ 0.1 of the mean pulse amplitude of a minimum ionizing particle. The discriminator values which are common to the four input channels can be set remotely from the central station. The high level outputs go to a programmable logic array (PAL) which forms the alert and trigger conditions. These conditions can be controlled from the central station and are normally set to ≥ 2 counters for the alert and ≥ 3 counters for the trigger. If the trigger condition is met, then a 5 mA current pulse of 5 μs duration is injected into the 50 Ω trigger request cable. (The flexibility in setting the alert and trigger conditions greatly assisted in experimentally establishing the optimum operating conditions for the array.) The alert pulse serves as the start pulse for the eight local TDCs, and is sent in the form of a TTL pulse over a 150 Ω twisted pair cable to each nearest neighbor station as a stop pulse in one of its TDCs. After passing through a lumped delay line the low level outputs are stop pulses for four of the TDCs. The start pulses from alerted nearest neighbor stations are received by an LT1016 comparator and serve as stop pulses for the four additional TDCs. The TDC circuit is similar to a previously published simple circuit using diodes as switches of a current source on to a capacitor [16].

Each TDC is calibrated by command from the central control. A pulse pair generation circuit employs a 50 MHz oscillator to inject start and stop pulses to each TDC. The oscillator was stable to better than 10 ppm in the interval 0°C to 60°C. The pulse pairs have time intervals which can be incremented in 20 ns steps to cover a 300 ns range. When digitized, each time channel corresponds to 0.3 ns. The charge from each PMT is integrated on a 470 pF polystyrene capacitor

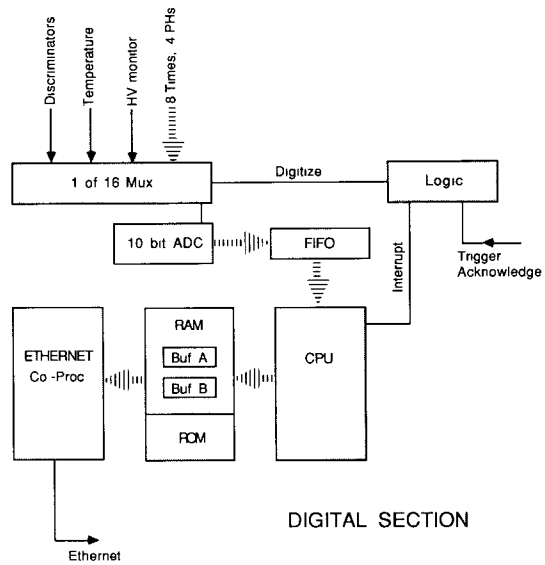

Fig. 6. Schematic diagram of the digital electronics.

and the value is sampled and held by a gate synchronized with appropriate time delay with respect to the formation time of the coincidence. When digitized, each channel corresponds to about 3 pC. The TDC values for the four local times, the TDC values for the four nearest neighbor times, the four pulse amplitudes, the PMT high voltage value, the ambient temperature, and the two discriminator settings are stored temporarily as 16 DC voltages waiting to be digitized if a trigger acknowledge pulse arrives.

Once a station alert occurs, an additional sequence of events begins which is controlled by another PAL. Further coincidences are inhibited while waiting for the receipt of a trigger acknowledge pulse from the central control. If no trigger acknowledge is received within 10 μs of the alert, then the TDCs and charge integrators are reset and the station is reactivated. The time that a station is inhibited is ~ 15 μs giving the dead time fraction of each station of ~ 0.2%.

A schematic view of the digital electronics is shown in Fig. 6. If a trigger acknowledge is received within 10 μs after an alert then the encoding of the data begins. The receipt of a trigger acknowledge advances an event counter in *every* station. The data are routed in turn to a single 10 bit ADC (RCA 3310) through a multiplexer. The rate of encoding is controlled by a 0.6 MHz oscillator. Sixteen cycles of this oscillator are required to encode each of the 16 DC voltages. The digitized data are passed to a FIFO memory which is controlled by the onboard Intel 80186 microprocessor (μP). The receipt of a trigger acknowledge inhibits all stations in the array. The total dead time for the entire array is about 0.5 ms while an event is being digitized.

The program for the onboard μP is stored in a 64 kByte EPROM. The μP is linked to the central station via the Ethernet communication protocol, which employs a local area network coprocesser (LANC). The μP receives instructions from the central station which can set the PMT voltage, the discriminator level, command a time calibration, or set the alert and trigger conditions. The μP transfers the data in the FIFO to the active half of a RAM and attaches additional status and event counter data. It also receives commands which control the data taking. Typically every 30 s the μP receives a command to switch the memory location to which the data from the FIFO are placed. At this point the final values of a software event counter, hardware event counter, and a free running millisecond clock are saved in the old buffer before being reset. Both the software and hardware event counter are advanced each time a trigger acknowledge is received regardless of whether the station was alerted. On a poll command to a station identified by its own unique Ethernet address the coprocessor sends the data in the inactive buffer to the central station. The data for each event consists of the 16 digitized voltages (32 Bytes) referred to above and an additional 8 Bytes giving the alert and trigger status of the station for the particular event, the software counter value, the hardware counter value, the reading of the millisecond clock and the Ethernet address. The software event counters are used to match events at the central station.

2.3. The central station

CASA is controlled by a Digital Equipment μVAX III$^+$ computer, located at the geometrical center of the array. This computer interacts with the CASA stations by two separate means: first, through a trigger box which is coupled to the μVAX by a DRV-11 parallel port and second, through an Ethernet system which connects the μVAX to all the CASA stations. The Ethernet link is used to control the operation of CASA and collect the data following local storage in the CASA stations.

2.3.1. Trigger box

Inputs to the trigger box are the trigger request line and a 64-wire parallel line which carries the value of a Global Positioning System (GPS) clock. This clock provides Universal Time which permits the reconstruction of a given event in astronomical coordinates. Outputs from the trigger box are: 1) the trigger acknowledge pulse which commands that data of the alerted CASA stations be digitized and, 2) a pulse which serves to stop the TDC's of the MIA muon counters. This pulse is generated with a fixed delay with respect to the leading edge of the first current pulse to arrive on the trigger request line.

The trigger box has a discriminator which fires when three current quanta overlap on the trigger request line. An important detail concerns the termination of the trigger request cable on a rib. For reasons of economy this cable was chosen to be RG-58 which for its 250 m length has DC resistance (20 Ω) which is significant compared to its 50 Ω impedance. Thus we chose to terminate this cable only at the repeater located at the junction of the rib and spine. Because of reflection from the open end, about 0.7 μs is required to reach a steady current in the termination resistor at the rib-to-spine repeater. The repeater fires on the leading edge of the first current pulse when a threshold of 1 mA is crossed at which time the pulse is regenerated on the spine cable. Therefore the time of arrival of the first pulse is preserved, and is not affected by its reflection. This time is essential in forming a narrow coincidence window between CASA and MIA. Subsequent current pulses on the same rib are regenerated on the spine only when the reflected part of the pulse arrives. Attenuation losses on the spine, which is RG-8, are small so that termination on both ends of its 500 m length is acceptable.

When the three quanta level is reached, the μVAX is interrupted and the trigger box is inhibited from receiving additional trigger requests. Then a trigger acknowledge is sent to all of the CASA stations. The trigger acknowledge signal is relayed from the spine to the ribs. The GPS time is latched by the μVAX and a trigger box event counter is advanced. After the GPS time is read, the trigger box is reenabled. The time interval during which the trigger box is disabled is less than the time for encoding the data in the alerted CASA stations so that it introduces no additional dead time. After a fixed delay beyond the arrival of the first of the $\geq$ three quanta, a stop pulse for the TDCs of the MIA muon counters is issued.

The trigger acknowledge output of the trigger box is also used for another essential purpose, the rebooting of the μPs in each CASA station. It is important to have the option of rebooting μPs at the beginning of a run because a few μPs can crash during a run. By the application of a sustained pulse train of 1% duty cycle on the trigger acknowledge line the μP can be rebooted. A circuit on the electronics board integrates the pulse train producing the appropriate reboot pulse.

2.3.2. The central control

The μVAX communicates with the μPs in each CASA station through a 1089 node Ethernet system. The system operates in a "master–slave" mode so that collisions of Ethernet packets are avoided during normal operation. As the array has grown in size the

Ethernet system has evolved. For economic reasons the Ethernet cables were chosen to be RG-58. We found that the maximum length of this cable for reliable operation was ~ 150 m. We have chosen a double spine system which is shown schematically in Fig 3. From the Ethernet transceiver on the μVAX the signals are conducted on optical fiber lines to east–west rows nine stations north and eight stations south of the central spine. At these rows the signal is transferred to RG-8 cables. The signal is then relayed to RG-58 cable on each half rib using commercial Ethernet repeaters [17]. A total of 68 such repeaters is used in the array.

The operation of the array is controlled by the μVAX. Each station is programmed to interpret commands from the μVAX over the Ethernet. Before a run is started all the CASA stations are rebooted. Then, one-by-one, each station is "verified"; a message is sent to each station which results in a response from the μP if the station is "alive". The PMT voltages, discriminator settings, alert condition and trigger condition are sent to each station. Then a command to start a calibration run for the TDCs is sent. After a time calibration run of several minutes, event data are collected for six hours. During a data run a command to shift the buffer is sent every ~ 30 s. Then, one-by-one, each station is polled for its data. The rate of triggers is 21–24 Hz, and the average event involves 19 alerted stations. With 1089 stations, a given station will have on average 13 events per poll. For simplicity we permit only one Ethernet packet in response to the poll which can contain a maximum of 36 events (1440 bytes). If a station is operating properly, the fraction of polls in which the station data overflows the memory is $\sim 2 \times 10^{-6}$. The time required for each poll is ~ 6 ms so that collection of the data from all 1089 stations requires ~ 6 s.

2.3.3. Sorting the data

After the μVAX collects the data from a poll, it proceeds to sort it into complete events. Here the sorting parameter is the station event counter. As a check of proper sorting the event counter in each station must agree with the trigger box event counter at the end of the poll. A station for which this condition is not satisfied is not included in the events of that particular poll. The next task of the μVAX is to merge the muon data from MIA with the CASA data.

3. The muon array (MIA)

The design of the muon array required a large shielded collecting area. The idea of burying the counters was chosen because of the relative ease and low cost of meeting the substantial shielding requirement. This forced extreme simplicity and durability in the counter design to ensure a useful life of at least ten years. A large counter size of 1.9×1.3 m was chosen. It works in a "digital" mode. The low muon density in airshowers in the 100 TeV energy range does not necessitate pulse height information. The "digital" nature also helped in developing a simple low-maintenance detector.

The construction of the muon counters has already been described [9]. Sixteen patches of sixty-four scintillation counters buried 3 m below the surface are located as shown in Fig. 1. The burial depth has been shown to reduce "punch-thru" of the electromagnetic component to an acceptable level [6].

The PMTs are EMI-Gencom type 9870B. They were sorted according to operating voltage by the following process. For each PMT we measured its efficiency for single photoelectron pulses to fire a discriminator with a 50 mV threshold. We increased the voltage on the PMT by 50 V steps and when the resulting increase in efficiency was less than 10% we stopped. Tubes that had a noise rate ≥ 10 kHz or required high voltages ≥ 3000 V were rejected. When the operating voltage was chosen in this way a typical counter was $\geq 98\%$ efficient for minimum ionizing particles. The efficiency of the counters when buried was measured to be 93% presumably due to some areas of optical contact between the scintillator and its wrapping due to the pressure of the over-burden. The signal and high voltage are carried on a single 75 Ω cable to each counter. For the more distant counters signal repeaters were installed to compensate for the attenuation in the cable.

The MIA electronics are located at the central station. The PMT signals are decoupled from the high voltage and pass to discriminators. The discriminated pulses serve as start pulses for a 1024 LeCroy Model 4290 TDC system which operates in a common stop mode. Only the arrival times of the muon signals are recorded.

The stop pulse for the muon TDCs comes from the CASA trigger box. This pulse has a fixed delay with respect to the time of arrival of the first CASA trigger request pulse as described above. Each TDC has 1024 channels of 4 ns width. The discriminators on the PMTs are set with a 5 μs dead time so that afterpulsing does not reset the TDC. The muon TDC values are read into a VAX 3200 computer along with the GPS clock time. The dead time due to the readout of the data is ~ 2 ms. The MIA computer has an Ethernet link with the CASA μVAX. The MIA data are merged with the CASA data and written to a disk on a poll by poll basis. The merging parameter is the GPS time of the event which is recorded by both data acquisition systems.

The singles rate of a typical muon counter is 6 kHz, of which 4 kHz is from radioactivity of the ground. The

PMT dark noise accounts for most of the remaining rate. With the 16 patches there are ~20 accidental counts during the 4 μs range of the TDC. As will be discussed in section 4.4, the construction of a narrow time window for definition of muons associated with the shower is crucial to obtain a good definition of muon poor events.

4. Performance of CASA-MIA

4.1. Trigger rates and accidentals

The trigger rate of the complete array is about 22 Hz at the average atmospheric depth of 870 gm/cm^2. This rate varies with the atmospheric pressure. The rate changes by 1% for a 1 gm/cm^2 change in air pressure. The average number of alerted stations is 19. Fig. 7 shows the frequency distribution of the number of alerted stations.

The 6.5 gm/cm^2-thick lead sheets placed on top of each station increase the trigger rate by a factor of 1.38. This indicates a reduction of the energy threshold for cosmic rays by a factor ~0.8. The addition of the lead also improves the angular resolution as will be shown in section 4.3.3.

A run was made in which the trigger request was generated by a pulse to determine the rate of accidentally alerted and triggered stations. For 31% of these trigger requests there was at least one accidental alert and for 2.6% at least one station trigger occurred. Most of these accidentals were due to a single station. About 0.02% of the accidentals were showers that would have generated a trigger request, consistent with the 10 μs time delay before an alerted station is reset and the 22 Hz trigger rate of the array. The effect of the accidentally alerted stations is not very important. It requires a small correction to the measured density

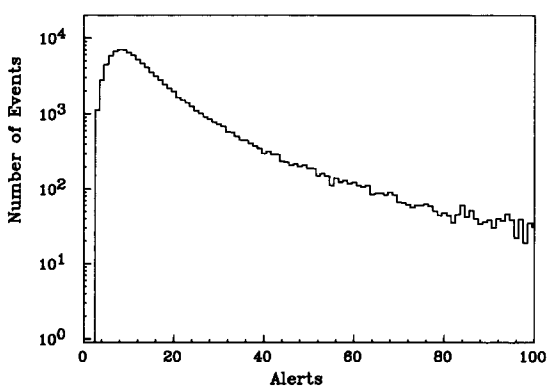

Fig. 7. Distribution of the number of alerted stations during a 6 h run.

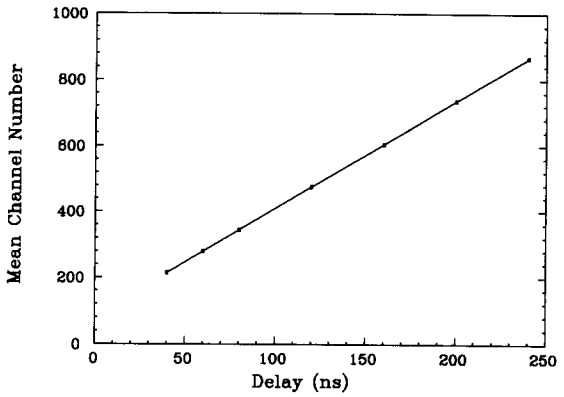

Fig. 8. Channel number vs delay between stop and start for a typical TDC.

of equivalent particles at a station (see section 4.3.4). The accidental station triggers, however, cause some problems with the determination of the coincident muons which will be discussed in section 4.4.

4.2. Calibrations

In order to reconstruct airshowers, the TDCs are calibrated by an internal oscillator, the gains of the counters are determined by the abundant cosmic ray triggers, and the cable and electronic delays are determined by the zenith angle distributions of the detected cosmic rays.

4.2.1. TDC calibration

A 50-MHz oscillator in each station can, upon computer command, inject into each TDC a series of start and stop pulses with a delay which is variable in units of 20 ns. A plot of channel number vs delay for a typical TDC is shown in Fig. 8. In the range of delays from 40 to 240 ns the relation is linear with a typical RMS deviation of 0.3 channels. These curves are fit to a form $T = AN_{ch} + B$, where T is the delay in ns and N_{ch} is the channel number. A typical value of the slope A is 0.31 ns/channel and the intercept B is −27 ns. The 50 MHz calibration oscillator has a temperature coefficient of less than 10^{-6}/C°. The temperature coefficient on the slope parameter is found to be either positive or negative depending on the particular station, the typical magnitude being 2×10^{-4}/C°. (The temperature coefficients are defined as the fractional change in the quantity per C°.) The temperature coefficient for the intercept is always negative with a typical magnitude of 1.8×10^{-3}/C°. The TDCs are calibrated at the beginning of each run which are typically six hours in length. Because the temperature variations in a given run can be as great as 25°C, the TDC calibration appropriate to the particular temperature at the

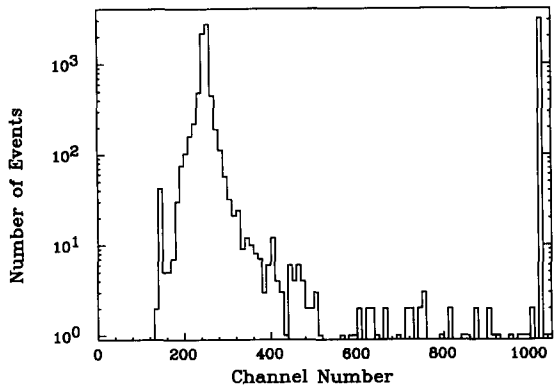

Fig. 9. Distribution of raw TDC channels for a typical counter.

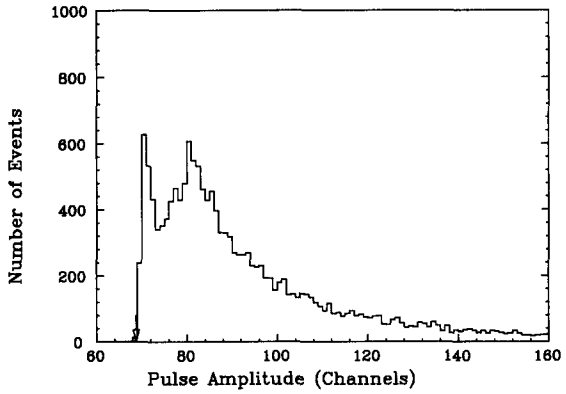

Fig. 11. Pulse amplitude distribution of the scintillator of Fig. 4 which satisfies the two-of-four condition (see text).

time of each event is used in converting from TDC counts to times in ns.

4.2.2. Determination of gains of each counter

The pedestals and gains for each of the four counters within each station are determined using the cosmic ray data. Fig. 9 shows the TDC distribution of a typical counter. There are two peaks, one between 200 and 300 channels, corresponding to the arrival of a shower particle in one of the counters that fired to alert the station, and one in channel 1023 corresponding to a counter that did not fire. Its time is measured with respect to the start determined by the coincidence between at least two of the counters.

Fig. 10 shows a plot of the value of the integrated pulse amplitude as digitized for events when the counter did not fire (TDC = 1023). In this manner the pedestal for each pulse amplitude measurement is established. Fig. 11 shows the distribution of pulse amplitudes for events with TDC values between 190 and 290 counts. This distribution was selected from events where only two of the four counters fired (two-of-four condition). This requirement enhances the number of events for which only a single particle passed through the counter. The pulse amplitude distribution plotted in Fig. 11 was obtained from the same scintillator as the plot of Fig. 4a. We recall that in Fig. 4a the pulse amplitude distribution for vertical muons as measured on the test stand was plotted. The peak at small pulse height is due to the soft photons in the shower.

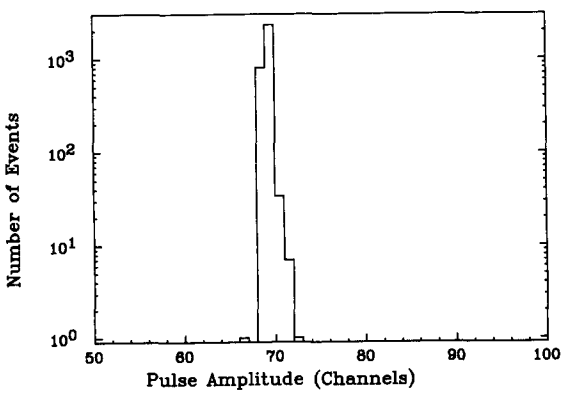

Fig. 10. Distribution of pedestals for a typical ADC.

A comparison was made between a representative set of counters each of which was measured in the field with the two-of-four condition and then measured on the test stand. For these measurements the test stand was included in the Ethernet link to the central station as all the stations in the array. In these comparisons the electronic board used was the same in the field as on the test stand. The gain of a counter is defined as the mean pulse amplitude after pedestal subtraction. The gain measured in the field with the two-of-four condition was found to be 1.48 ± 0.05 times the gain measured on the test stand for vertical muons. When the lead converter was removed the factor was found to be 1.21 ± 0.05. Thus by measurements in situ the gain of each counter for a vertical muon can be determined. The high voltage of each set of four counters is adjusted so that the two-of-four gain is about 30 channels. Considering the gain ratio 1.48, the gain of each counter for a vertical muon is about 20 channels. A counter with a gain of 20 on the test stand was determined to have an efficiency of $\geq 99\%$ for vertical muons. The setting of the upper level discriminator corresponds to a threshold of approximately 2 channels as shown in Fig 4a. The number of equivalent particles detected by a counter in an individual event is defined as the observed pulse amplitude divided by the gain of the counter for a vertical muon.

4.2.3. Internal offsets

While the cable lengths of each scintillator to the electronics are equal in a given station, there are

offsets in the mean time difference measured between any pair of counters. Physically all these differences should be zero; any systematic difference represents an offset due to different delays in the electronics. These differences are called the internal offsets (IOs).

Before these offsets are determined, a slewing correction, established from the data, is made. These corrections are made before the raw TDC channels are converted to ns and are given by the following:

$\Delta_t = -350/(10 + PA)$ for the 10 stage tubes.

$\Delta_t = -300/(10 + PA)$ for the 12 stage tubes.

Here PA is the pedestal subtracted pulse amplitude measured in channels and Δ_t is measured in TDC channels.

Once the slewing corrections are applied the times of each counter are converted to ns and the distributions of the six possible time differences are made. These distributions typically have an RMS width of ~ 1.8 ns. If the delays in the PMTs, cables, and electronics were identical in all four channels then all these distributions would be centered at zero. The internal offsets (IOs) are defined as subtractive constants so that the centers of the time differences are all corrected to zero. Thus the final corrected time of a counter is given by:

$T(\text{corrected}) = T(\text{raw}) - \text{IO}.$

There are three IO constants for each station. (The IO of the north-west counter in each box is arbitrarily set to zero.) The typical values of the IOs have an RMS spread of 1.8 ns and a mean of -0.7 ns. The IOs are calculated for each run. We have verified that the values of these constants averaged over a run with a large temperature variation give the same results as evaluating the constants as a function of temperature over several runs.

4.2.4. External offsets

Each station of CASA is linked to its four nearest neighbors by two twisted pair cables. On one of these cables the start pulse of the station is sent to the nearest neighbor as a stop pulse. On the other cable the start pulse of the neighbor is received as a stop pulse for the local TDC. This exchange of time signals permits the measurement of the difference in arrival time of the shower between the two stations. When two adjacent stations are both alerted they are defined to be linked.

The time of the first counter to fire is taken as the best measure of the arrival of the shower front at the station. We denote this time for the ith station as T_i. We denote the start time as T_i^0. Then the local time measured by the TDC is:

$\tau_i = T_i - T_i^0.$

The time from a jth neighbor (called *crosstime*) is measured by the TDC to be:

$\tau_{j,i} = T_j^0 - T_i^0.$

Using similar notation for the jth station with its crosstime from the ith station one finds that the time difference for the arrival of the shower front is given by:

$T_i - T_j = \tau_i - \tau_j + (\tau_{i,j} - \tau_{j,i})/2.$

The result is independent of the individual start times of each TDC. The error in the time difference measured between adjacent stations is dominated by the time jitter of the PMT signals and it is ~ 1.7 ns.

It can be shown with the above expressions that the sum of the crosstimes is a constant. This sum is an excellent check of the proper functioning of the electronics. The typical RMS of this sum is 0.2 ns and is a measure of the intrinsic jitter of the electronics. The net time difference between two alerted stations separated by N links can be determined by summing the time differences of each of the linked stations. It can be shown with the above equations that this time difference has an additional error of only $\sim 0.2\sqrt{N}$ ns. The time jitter of each of the intervening stations cancels out and only the intrinsic electronic jitter remains.

Fig. 12 shows the TDC distribution for a typical crosstime channel. The broad spread of the TDC channels is due to the angular distribution of the cosmic ray directions. Fig. 13 shows a plot of $T_i - T_j$ for a pair of stations. If all the delays in the electronics and cables were equal, the distribution would peak at zero for the case of the two stations being in a horizontal plane. The external offsets (EO) are defined to account only for the inequalities in the electronics and cable delays. Thus the difference in the vertical height of the stations must be taken into account so that cosmic rays from the zenith will appear at zero in a plot for the

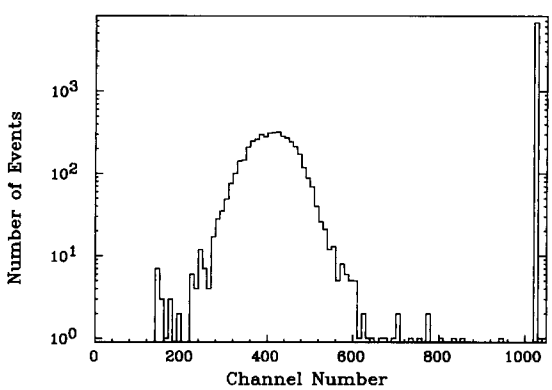

Fig. 12. TDC distribution for a crosstime channel.

corrected time differences. The $EO_{i,j}$ are thus defined as the displacement of the peak of the distribution of $T_i - T_j + (n_z/c) \times (h_i - h_j)$ where h_i is the vertical height of the ith station measured with respect to a reference plane and n_z is the direction cosine of the cosmic ray direction with respect to the vertical axis. Here c is the velocity of light, 0.3 m/ns. Since n_z is not known a priori we take its average value 0.91 in plotting the distribution. The RMS width of this curve is typically 16 ns. In a run of six hours about 4000 events are accumulated for each difference so that each external offset is determined with a precision of ~ 0.3 ns. The temperature variation of these offsets is such that no significant error is introduced even when there is a large variation in temperature during a run. The height corrected absolute time difference $D_{i,j}$ is given by:

$$D_{i,j} = T_i - T_j + n_z/c(h_i - h_j) - EO_{i,j}.$$

The values of the EOs on average are zero with an RMS spread of 4.3 ns about zero. The value $D_{i,j}$ is directly related to the direction cosine along the direction joining the ith and jth stations. If this is the x direction then n_x is given by:

$$n_x = cD_{i,j}/(X_i - X_j),$$

where X_i and X_j are the respective X coordinates of the stations.

4.3. Reconstruction of the showers by CASA

Reconstruction of the core position, direction, and size (number of equivalent particles) of each shower is done using the calibrated data. The position of the core of the shower is determined from the number of equivalent particles observed in each station. The direction of the shower is determined from the time differences measured between linked stations. The mean number of links is 7 in each orthogonal coordinate. The time of arrival of the shower front at a station is normally taken to be the time of the first counter that fired after correction by the IOs. (In cases where the pulse amplitudes are large a more complex algorithm using times from several counters may be used to define the shower front.) Unlinked stations are only useful in the size determination of the shower. In Fig. 14 we show two-dimensional histograms of the equivalent number particles in each station and the relative times of arrival of the shower front at each station for a typical event. From these data the direction and size of the shower are reconstructed. By size we mean the total number of equivalent particles in the shower.

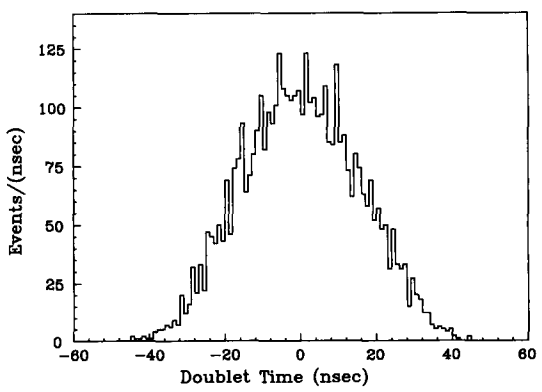

Fig. 13. Plot of time difference between two stations (doublets) before subtraction of the external offset and correction for the difference in height of the two stations.

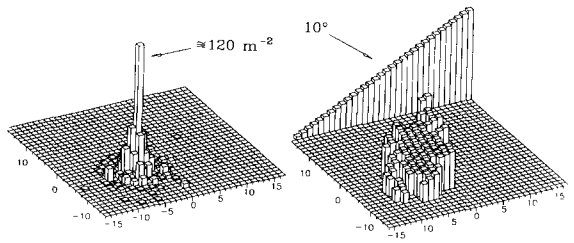

Fig. 14. Lego plot of the particle density of a typical shower (left). Lego plot of the relative arrival times of the same shower (right).

4.3.1. Reconstruction of the core position

The core of the shower is the point where the extrapolated trajectory of the primary particle would have hit the ground. It is the point of highest density. For 70% of the showers the core can be accurately located by the center of gravity of the five stations with the highest shower particle density (HIGH5 method). The weight of each station is the estimated number of particles summed over the four counters. If some of the stations are saturated (number of particles ≥ 100), then the weight of the saturated stations is taken as a constant equal to the lowest saturation level. The HIGH5 method is supplemented by a technique (CIRCLE-CORE method) which exploits the fact that the lateral distribution in the shower plane is azimuthally symmetric about the core. If ≥ 3 stations can be found with the equivalent number of particles greater than 7.5 (density $= 5/m^2$), then isodensity circles are constructed which are centered on the core location. Isodensity points are found by interpolating between stations and ≥ 5 points are required for a contour fit. The CIRCLE-CORE method is used in preference to the HIGH5 method when possible. The CIRCLE-CORE method can locate cores which fall outside the array.

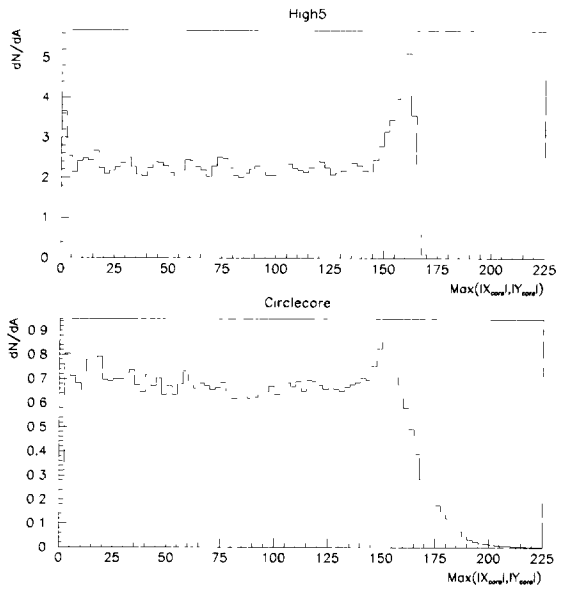

Fig. 15. Density of reconstructed core locations as a function of the half-size of a square annulus. For the HIGH5 method (above). For the CIRCLE-CORE method (below).

In Fig. 15 we show the distribution of core locations as a function of the maximum value of the cartesian coordinate (either X or Y) of the reconstructed core. The coordinate origin is the center of the array. These studies were done when the array contained 529 stations with the edge at 165 m from the center. Two curves are shown. Fig. 15a shows the distribution for the HIGH5 method. There is a peak at the edge corresponding to cores "pulled in" because the method has no means to construct a core outside the array. Fig. 15b shows the result of the CIRCLE-CORE method when conditions permit its application. Here the distribution of cores extends outside the array. It falls off smoothly as larger and larger showers trigger the array beyond its boundary. Care is taken to eliminate gross errors caused by large density fluctuations of distant big showers and by various hardware malfunctions.

The accuracy of the core location has been evaluated by Monte Carlo simulations and by checking self-consistency of the reconstruction algorithm when an artificial edge of the array is introduced. The core reconstruction precision improves as total number of detected equivalent particles increases. The precision of the core reconstruction (except within 15 m of the edge) is typically better than 3 m and is shown in Fig. 16 as a function of the total number of equivalent particles.

4.3.2. Reconstruction of the direction of the shower

Accurate reconstruction of the shower direction is essential for the application of an airshower array to gamma ray astronomy. Rejection of the cosmic ray background improves with improving resolution; the signal to noise for the detection of a point source is inversely proportional to the resolution. The station offsets were determined so that the direction of the zenith is defined by the maximum yield of the cosmic rays. The conversion of the measured time differences between stations to a zenith angle depends on the calibration of the TDCs by the local oscillator in each station. The survey of the array which determined its orientation with respect to north determines the origin of the azimuthal angle scale.

The determination of the direction cosines of the shower axis requires an iteration to account for the difference in the elevation of the linked stations. If T_i and T_j are the corrected times for two linked stations on the x-axis then the direction cosine n_x is given by:

$$n_x = c\frac{(T_i - T_j)}{(x_i - x_j)} - n_z\frac{(h_i - h_j)}{(x_i - x_j)}.$$

A similar expression holds for n_y. Since one does not know a priori n_z, we begin with the average value of $n_z = 0.91$. Once n_x and n_y are computed, a more accurate value of n_z can be inserted, and then n_x and n_y are recalculated. The overall direction cosines are averages of the values obtained from the individual links weighted by the sum of the equivalent particles detected in the two stations forming the link.

The precision of the direction cosines is improved in a second step. For most events the number of measured time differences (i.e. the number of links) is larger than the total number of linked stations. For example, if 25 stations in a 5×5 array are hit there are 40 links for which 24 relative times need to be determined (the time of one station may be chosen arbitrarily). Using the station nearest the core as a reference,

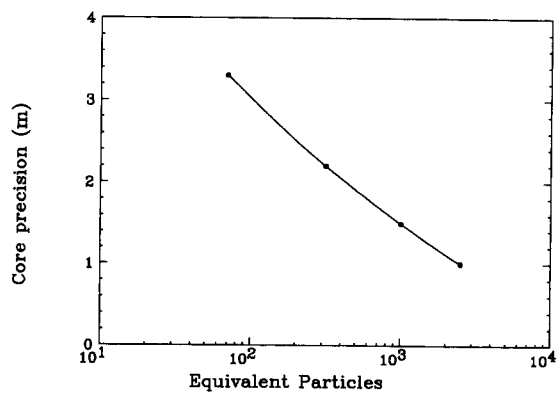

Fig. 16. Precision of core reconstruction as a function of number of detected particles. The precision is defined as the average absolute difference of the reconstructed core position and the true position.

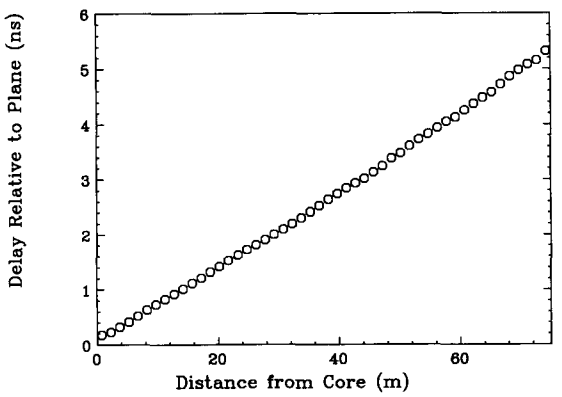

Fig. 17. Plot of the shower front as a function of distance showing its conical shape.

the relative arrival times of the shower at all the linked stations are determined using all the available time information.

Using the relative times, the relative heights of the stations, and the direction cosines from the first pass, a plane shower front can be constructed. A large sample of showers were fit to planes. The residuals to this fit are plotted in Fig. 17 as a function of the distance from the core. The residuals are well fit with a slope of 0.07 ns/m which implies that the shower front has a conical shape.

In the final determination of the direction cosines a fit to the conical shower front is made. In the fit each station time is assigned an error, empirically determined from the residuals, given by

$$\sigma_t^2 = \left(1.6^2 + 3.0/N_a\right)\left(1 + R_c/60\right)^{1.3}\ \text{ns}^2$$

where N_a is the number of equivalent particles detected in the station and R_c is the distance from the core in meters.

4.3.3. Angular resolution and absolute precision of the shower direction

To be confident of astronomical results, which may be only upper limits on source fluxes, it is crucial that the direction of each air shower is properly reconstructed and that the point spread function of the instrument is well understood. To date we have observed no γ-ray source which we might be able to use to confirm the pointing and to calibrate the resolution. We have thus resorted to a number of indirect techniques to study the resolution and the pointing accuracy. We define the resolution as the angular radius that would contain 63% of showers coming from a point source (σ_{63}). This is a useful definition because it describes a solid angle which is close to optimum for maximizing a signal from a point source on a uniform background. If the resolution function can be approximated by a two-dimensional Gaussian, then σ_{63} is $\sqrt{2}$ times the standard deviation. The definition of σ_{63} is, however, independent of the particular shape of the resolution function.

For the following discussion we express the resolution as a function of the total number of alerted stations. Statistically, the most powerful method to determine the resolution is the "split-array" method which makes use of the cosmic ray data. For each station we divide the four counters into two separate pairs and treat each pair as an independent station. Timing signals are considered for each pair; effectively we have two sub-arrays, each with half of the detector area of the original array. For a given shower the direction is measured by the two sub-arrays and the difference of the two space angles is determined. If the two sub-arrays were totally independent one would divide the difference distribution by $\sqrt{2}$ to get the distribution of each sub-array with respect to the true direction. Then, since each sub-array has half the area of scintillator, we might estimate that the precision in angle would be $\sqrt{2}$ worse, so that σ_{63} is 0.5 times the space angle difference that contains 63% of the events. However, because timing signals between links are shared by both sub-arrays they do not operate as completely independent arrays. We have calculated by simulation the factor by which the observed spatial angle containing 63% of the events must be multiplied to obtain the angular resolution. The simulation includes the arrival time distribution of the air shower particles together with the 1.2 ns instrumental time resolution for each counter. This factor varies from 0.50 for small showers (alerts ≤ 10) to 0.95 for large showers (alerts ≥ 100). Fig. 18 shows σ_{63} determined by the split array technique as a function of the number of alerts.

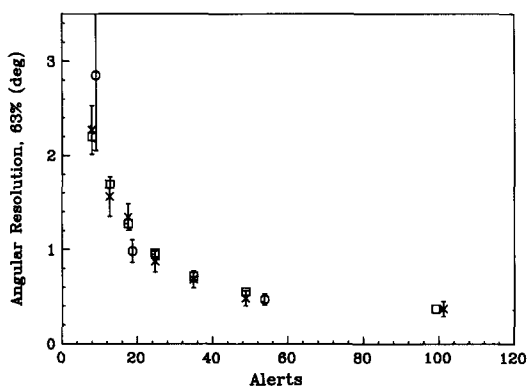

Fig. 18. Resolution of CASA as a function of the total number of particles. The squares are the split array method, the crosses are from the Cherenkov telescopes, and the open circles are from the shadow of Moon. The dotted line is an overall fit.

We have evaluated the improvement in angular resolution gained by placement of the lead above the station. With the split-array method we calculated the ratio of the angular resolution with and without lead as a function of the number of muons detected in the shower. (The discussion of the muon detection is given in section 4.4.) The number of muons is unaffected by the lead so that the ratio shows directly the improvement produced by the lead for showers of identical size. We find the ratio of the angular resolution with the lead to that without to be 0.74 ± 0.03 independent of the number of muons.

Although the split-array method permits a calculation of σ_{63} as a function of alerts with very small statistical error, it cannot evaluate a possible systematic error in the reconstruction of the direction of the shower. It also depends to some extent on simulation. We therefore used a second technique which measures both the absolute pointing of the array and σ_{63}. There are five small telescopes that were built by the University of Utah to search with the atmospheric Cherenkov technique for point sources emitting γ-rays [18]. Each telescope consists of a single 5-cm PMT at the focus of a 35 cm diameter steerable mirror. Four telescopes are located 120 m north, south, east, and west of the center of CASA. A fifth telescope is located at the center of CASA. The threshold of these telescopes matches that of CASA rather well; about 50% of the telescope triggers in the 6° diameter field of view have a coincidence with CASA. The direction of the shower observed by the telescopes is determined by the time of arrival of the Cherenkov light. The direction of pointing of the mirrors is verified by the observation of a number of stars. We have recorded about 10000 coincidences between CASA, operating with 1089 stations and the telescopes, aimed toward the zenith. The resolution of the telescopes (when at least four of the five were hit) was found to be $\sigma_{63} = 0.65 \pm 0.05°$, independent of the size of the shower. Using this subset of the data, σ_{63} for CASA was calculated and is also plotted in Fig. 18. The agreement between the two methods is excellent. We find σ_{63} averaged over the entire data set is $1.16 \pm 0.05°$. However in the search for point sources, greater sensitivity can be obtained using the knowledge of the resolution as a function of number of alerts.

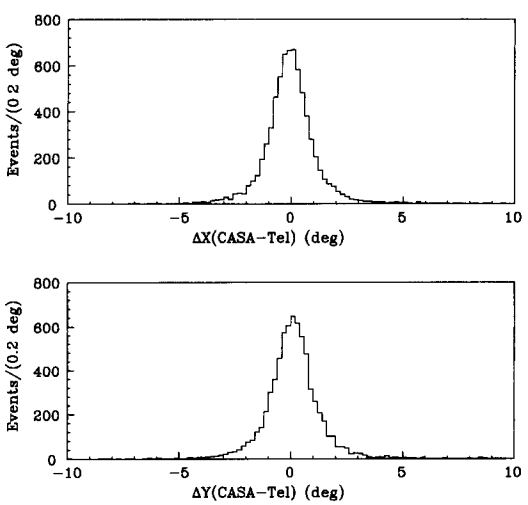

Fig. 19. Comparison of directions determined by CASA with the directions determined by the Cherenkov telescopes. Difference of angles projected along the x-axis (above). Difference of angles projected along the y-axis (below).

The telescopes also were used to verify that there are no systematic errors in the reconstruction of the shower direction. In Fig. 19 we plot the projected angular differences between CASA and the telescopes. The mean offsets are found to be $-0.064 \pm 0.02°$ and $0.068 \pm 0.02°$ for the x and y directions respectively. Similar offsets were found for the telescopes directed away from the zenith when CASA was operating with 529 stations. These data show that the systematic error in the direction reconstruction is less than 0.1° for the full range of zenith angles accepted by CASA.

Finally, we can use an astronomical body to verify the pointing accuracy and the angular resolution. The Moon is opaque to the cosmic rays passing through the solar system. Thus we expect to see the shadow of the Moon in the midst of the isotropic distribution of the cosmic rays. (The Sun can be observed as well, however, the position and shape of its shadow is affected by the magnetic fields which surround it.) The number of events available for this study is limited because the Moon subtends an angular diameter of only 0.5° and appears at relatively large zenith angles. Nevertheless, the detection of the Moon's shadow is a complete test of the performance of the array from input data to final result.

In Fig. 20 we present the shadow of the moon in cosmic rays. The radial bins are centered on the position of the Moon and the bin widths are chosen contain equal solid angles. The dashed line is the distribution expected in the absence of a shadow. From these data we establish that the pointing accuracy of the array is better than 0.2° at zenith angles of $\sim 30°$. The value of σ_{63} obtained from this study for separate ranges of alerts is also plotted in Fig. 18. A separate paper on the details of this study of the sun and moon shadow is in press [19].

4.3.4. Measurement of the density of shower particles at a station

To reconstruct the lateral density distribution and, by integration, the size of a shower we need to know the number of equivalent particles detected at each

station. As noted above, the number of equivalent particles recorded in an individual counter is given as the ratio of the observed pulse amplitude to the mean pulse amplitude for a vertical muon. In principle the number of equivalent particles hitting a station is just the sum of those found in each counter. There are complications, however, due to the resolution of an individual counter, the saturation at large pulse amplitude, and the alert condition when the number of particles is less than a few. As indicated in section 2.1, at least two of the four counters must be hit in coincidence to alert a station and record the data. If only one of four stations is hit, the station is not alerted and the data are not recorded.

If N particles are incident on a station, the probability of all N hitting only one counter is $(0.25)^{N-1}$. Thus for four or more particles the chance that a station is not alerted is negligible and the sum of the particles hitting each counter is the best estimate of the number hitting the station. The fact that four counters are combined improves the resolution. The ADCs have a dynamic range of about 950 channels, taking into account the pedestal at ~ 70 channels. Typically the mean channel number for a single equivalent particle is 20 channels above pedestal so that saturation occurs at ~ 45 particles. In fact because of the pulse height resolution the saturation begins a bit earlier. The resolution which is about 100% for a single particle improves as $\sqrt{N}$ for N particles. Using the experimental resolution given in Fig. 4, we have calculated the response of a station as a function of the number of particles incident upon it vertically. We assume that the gain of each counter is the same and

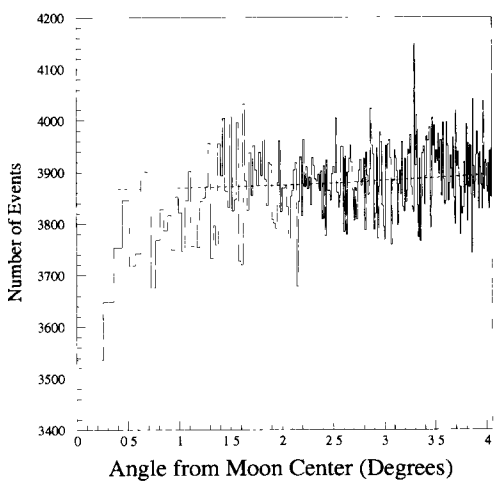

Fig. 20. The shadow of the moon as seen with cosmic rays. The bin widths correspond to equal solid angles. The dashed line is a fit to the distribution of events derived from the data without a shadow.

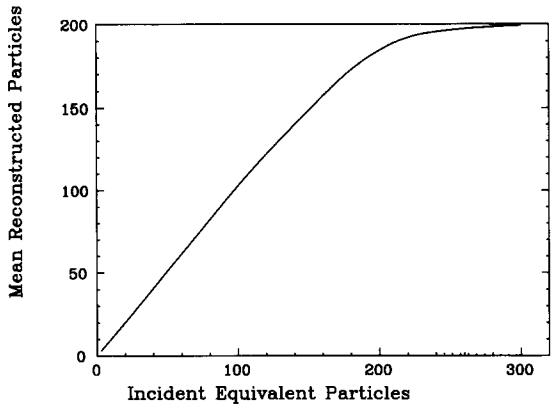

Fig. 21. Mean number of equivalent particles determined in a station as a function of the number of incident particles (solid line). The RMS fluctuation in percent of an individual measurement (dotted line).

that there are no short distance correlations between the particles. Fig. 21 shows the response of the station. Plotted are the means and the standard deviations. Actually the response of each station will have somewhat different saturation points depending on the individual gains of the counters which are not always balanced. The stations can usefully record up to ~ 180 equivalent particles, a density of ~ 120 particles/m^2. The saturation of a station occurs at lower densities when the showers have a significant inclination.

When the mean number of particles is less than ~ 4 we can use a statistical method to estimate the number of particles. If the mean number of particles incident on a station is N, then the probability that a counter *not* be hit is $p = \exp(-0.25\ N)$. In terms of p, the relative probability P_i of i counters being hit can be calculated. Since an alert requires two counters to fire, an ensemble of stations expected to have the same density can provide the relative probabilities $(P_0 + P_1)$, P_2, P_3, and P_4. The probabilities P_0 and P_1 are summed because experimentally they are indistinguishable. These probabilities can then be used to calculate the most probable number of particles incident on the station.

At low particle density the production of a station alert becomes very inefficient because at least two counters must be hit. This situation permits a direct comparison between the observed number of particles as measured by the pulse height (*analog particles*), and the number of particles measured by the statistical method (*digital particles*). We discuss here the density measurement without the lead converter. The lead converter changes the relative probabilities by the addition of a short distance correlation between particles which can be neglected when the lead is not present.

The measurement of the density with the lead converters will be discussed in a future paper.

A special run containing 150000 showers was made with the lead converters removed. A subset of 40000 vertical showers ($\cos\theta_z \geq 0.95$) with cores ≥ 45 m from the edges of the array was selected for study. These showers were then sorted into categories according to the number of alerts associated with each shower. We have chosen to study showers with 19 or 20 alerts, a category which corresponds to the mean number of alerts recorded by CASA. About the core position of each of these showers, annuli of width 5.0 m were constructed. Then sums of the number of stations (N_t), the number of stations with two counters hit (N_2), three counters hit (N_3) and four counters hit (N_4), and the total number of equivalent particles (Ph_t) were made for *all* the showers for each annulus. The mean number of analog particles N_a striking each station in a given annulus (given distance from the core) is given by Ph_t/N_t. The mean number of digital particles N_d striking each station is given by:

$$(2\times N_2 + 3\times N_3 + 4\times N_4)/N_t.$$

In Fig. 22 we plot the ratio N_a/N_d as a function of distance from the shower core. At ≥ 100 m from the core this ratio is 0.96. The ratio rises for distances below 100 m because N_d saturates at 4.0 while N_a saturates at ~ 180 particles. The fact that the ratio is close to unity means that our calibration of an analog particle agrees with the digital measurement when the density is low. This fact permits us to calculate the mean number of equivalent particles that pass through each detector but remain undetected due to the alert condition which requires at least two counters to be hit. If we assume the fluctuation of the number of particles in an annulus is governed by a Poisson probability, it is a simple matter to compute the value of N_1/N_t and derive a correction factor between the

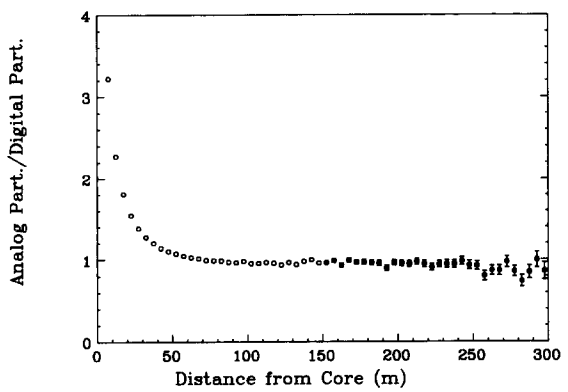

Fig. 22. Ratio of the number of equivalent analog particles to the number of digital particles.

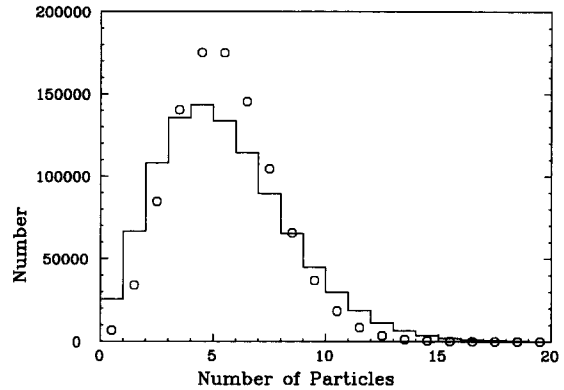

Fig. 23. Fluctuations in the number of particles striking a station with a mean of 5. Poisson distribution (circles). Distribution modified to match the observed counter multiplicities (histogram).

mean number of analog particles observed and actual mean number of particles. We find however that the relative numbers P_0+P_1, P_2, P_3, and P_4 are not consistent with a Poisson distribution when taken at a fixed distance from the core for an ensemble of vertical showers characterized by a fixed number of alerts. The relative numbers are better accounted for if we consider fluctuations somewhat larger than that of a Poisson distribution. These larger fluctuations may be due to a number of factors which include larger intrinsic fluctuations, the effect of finite annulus size, and spread of shower size for a fixed number of alerts. In Fig. 23 we plot, for a mean value of five particles striking a station, the Poisson fluctuation and a broader distribution which gives better agreement for the observed values of P_t. The correction factor for the lost particles due to the trigger condition is, however, nearly independent of whether the fluctuations are Poissonian or wider. In Fig. 24 we plot the correction factor for both

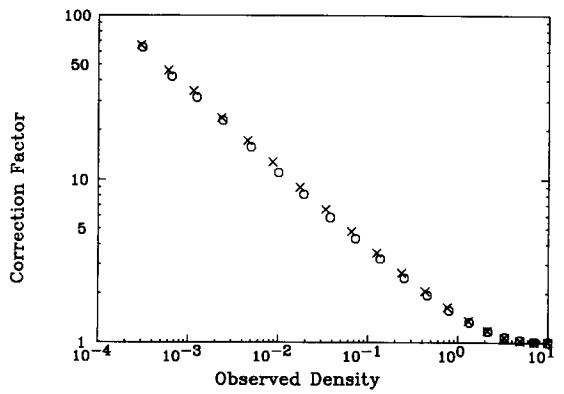

Fig. 24. Correction factor for analog particles lost due to the alert requirement. Circles are for the modified distribution. Crosses are for a Poisson distribution.

the Poisson distribution and the wider distribution. This correction factor is most useful when applied to an ensemble of showers selected to have similar properties.

As an example we have determined the average lateral distribution of the selected vertical showers which have 19 or 20 alerts. This range corresponds to the average shower detected by CASA. The mean number of equivalent particles is evaluated for each annulus. After subtraction of 0.00045 ± 0.00005 equivalent particles to account for the accidentally alerted stations (see section 4.1), the mean number is multiplied by the correction factor of Fig. 24. The resulting lateral distribution of density of equivalent particles is plotted in Fig. 25. The errors at large distance from the core are due to the uncertainty in the accidental subtraction. The integrated size in terms of equivalent particles within 300 m from the core is 2.44×10^4. Plotted on the same figure is the result for the MOCCA [20] simulation for an average 10^{14} eV proton shower. In the simulation we calculated the lateral distribution of equivalent particles, electrons and muons, which would be recorded by CASA scintillators. Before plotting, the simulation was multiplied by a factor 0.94 to match the integrated size of the data.

The above analysis was applied to ensembles of many showers with common characteristics. Such analysis provides input for algorithms for the reconstruction of the size of individual showers. Discussion of these details and the more complex treatment for the lead converter will be reported in subsequent papers.

4.4. Measurement of the muons associated with the shower

The primary purpose of the muon detector system is the identification of candidate γ-ray showers and the rejection of background hadron showers based upon their muon content. Several calculations predict that in the energy range 10^{14}–10^{15} eV, γ-ray showers will generate ~ 30 times fewer muons than hadron showers [21]. The underground scintillation counters sample air shower muons by recording muon hits that are coincident with the arrival of the electromagnetic component of the shower detected by the CASA surface array. Showers with significantly fewer detected muons than expected are considered candidate γ-ray showers. The remaining showers are considered hadronic background, and are thus rejected in searches for gamma ray sources.

The MIA system records all hits to underground muon detectors during an interval of ~ 4 μs coincident with the detection of showers by the CASA surface array. This time interval is large enough to include muon hits from showers arriving from any direction incident on any location of the array. However, the

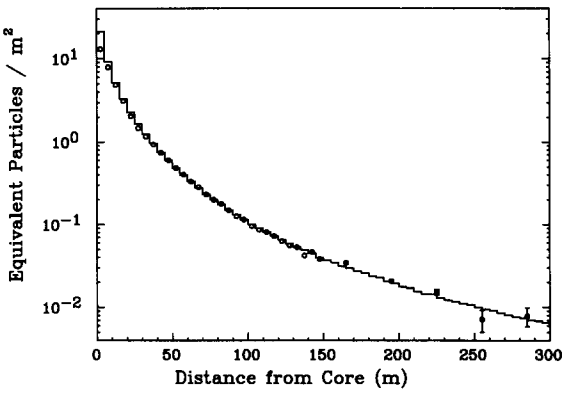

Fig. 25. Lateral distribution of equivalent particles determined from an ensemble of vertical showers with 19 or 20 alerts (circles). Lateral distribution of equivalent particles as determined by the MOCCA simulation for 10^{14} eV vertical showers (histogram).

number of accidental muon hits during this interval is large compared to the number of real muon hits in each event. On average, the number of muon counters that fire accidentally during this interval is about 20, while the average number of real muon hits from each air shower is only 9.

We can greatly reduce the effect of accidentals by taking advantage of the timing characteristics of arriving muons. Real shower muons will arrive within a tightly constrained time window associated with the physical width of the shower front, while accidental muon hits are distributed randomly throughout the 4 μs interval of the muon TDCs. By narrowing the time interval for the acceptance of muons, we can greatly reduce the number of accidental muon hits associated with the showers. We accomplish this by determining the anticipated arrival time of muons at each individual muon counter using the reconstructed shower from the CASA surface array.

Timing coordination between the muon counters and the surface array is provided by the common stop from the CASA trigger box. The common stop is associated with the arrival of the first trigger request current pulse at the central trigger box. For each event, current pulses from at least three individual CASA stations will arrive at the central trigger. The first such pulse to arrive is called the "first trigger". The cable delays for the transmission of current pulses from each CASA station to the trigger box have been directly measured. Using the core position and the direction cosines of the shower as reconstructed from the surface data, we can identify the particular CASA station that provided the first trigger for each shower. We define the time of passage of the shower front through that station as a zero time reference for the entire event. With respect to this zero, the shower front

passes a given muon counter at a time T^{μ} which can be computed from the shower parameters and the location of the particular muon counter. Note that this time can be negative (late) or positive depending on the direction of the shower.

When a muon counter is hit, the signal starts a TDC for that counter. The start of the particular muon TDC is at $T^{\mu} + T^{\mu}_{\text{cable}}$, where T^{μ}_{cable} is the time delay in the cable from the muon counter to its TDC. The stop of the TDC is at a time $T^{e}_{\text{cable}} + T_{\text{stop}}$ where T^{e}_{cable} is the known delay between the first trigger CASA station and the trigger box and T_{stop} is the delay between the arrival of the first CASA trigger and the common stop of the muon TDC system. This latter delay is a constant.

As with the surface array, the muon array can be calibrated using the cosmic ray events themselves. We measure the average value of $T^{\mu}_{\text{cable}} + T_{\text{stop}}$ for each muon counter with respect to all first trigger CASA stations. This is given by:

$$T^{\mu}_{\text{cable}} + T_{\text{stop}} = \langle \text{TDC}^{\mu} + T^{\mu} - T^{e}_{\text{cable}} \rangle .$$

Here TDC^{μ} is the measured TDC value for the particular counter. The average delay measured includes the delays in the muon counter PMTs and in the electronics. The spread of this measurement (~ 10 ns) around its average value includes the effects of errors in reconstruction of the shower, fluctuations in the arrival time of muons with respect to the shower front and variations in the PMT delays and electronics of each first triggered station used in the average. Once the delay for each muon counter is determined, a similar procedure is carried out for each first triggered station to determine the station offsets. These offsets vary by ~ 10 ns. Both muon and station offsets are then applied as a correction to the TDC of each muon counter so that the mean arrival time is zero. Fig. 26 shows the distribution of these corrected muon times.

The residual time spread in the muon hits as shown in Fig. 26 is due to the intrinsic spread of the muon shower front but more importantly, it is also due to the manner in which the muon timing is established. Since the muon time scale is determined by the surface shower parameters, an error in either the reconstruction of the shower direction or in the identification of the first trigger CASA station can result in large errors in the muon times. If uncorrected, such errors may lead to the misidentification of showers as muon-poor, since the associated muon times are pushed out of the narrow coincidence window. Even if these timing errors are rare, they can easily limit the muon rejection obtainable for large showers.

To investigate the impact of muon timing errors, we study events with large numbers of muon hits so that the timing can be reconstructed independently of the surface array reconstruction. For $\sim 1\%$ of the events

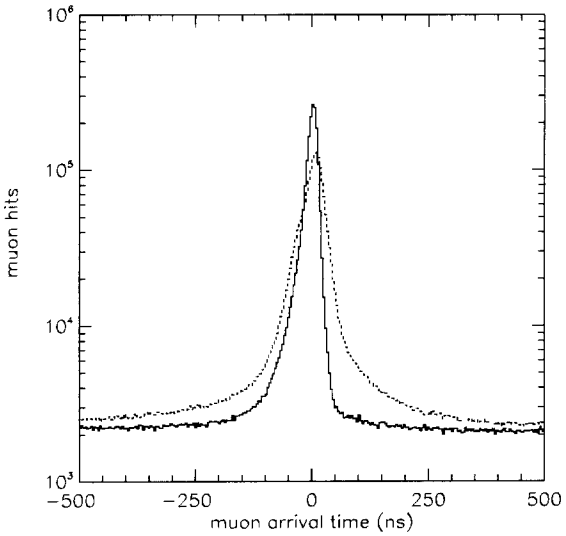

Fig. 26. Distribution of muon times with respect to the shower front, correcting for offsets (dashed histogram). Distribution of muon times corrected with the cluster algorithm (solid histogram).

with a large number of muons, the muon times are displaced significantly from the calculated zero arrival time. We find that a small fraction of the timing errors result from unrecognized cases where a CASA shower is incorrectly merged with an uncorrelated MIA event, or, in the early days of operation, from hardware problems. However, most muon timing errors are caused by small air showers that can initiate individual station trigger pulses either just before or just after a regular air shower event occurs. These accidental station triggers, discussed in section 4.2, are caused by real air showers that are too small to satisfy the three-station threshold required for an array trigger, but provide enough particles to cause one or two CASA stations to form a station trigger.

When an accidental station trigger occurs in isolation, the trigger box simply resets, and there is no adverse impact on the muon timing. However, if the accidental trigger occurs within the 4 μs TDC range of a real array trigger, it can cause a shift in the global time base for that event. In the case that the accidental shower occurs *before* the real shower, the charge pulse from the accidental station will arrive earlier than the real first trigger associated with the real shower. As a result, the muon TDCs will be stopped too early. If the accidental trigger arrives *after* the real shower, then the accidentally triggered station may be incorrectly identified as the first trigger station, depending upon the geometry of the event (e.g., in the case that the real shower core is located near the edge of the array and the accidental station is located near the center of the array).

Although the muon timing errors that result from first trigger misidentifications can be very large, the timing shift is identical for each muon TDC in a given shower. Therefore, the times for real muon hits should remain tightly clustered, even if the global time base is corrupted. To compensate for the effects of misidentified first trigger stations, we have developed an algorithm to identify clusters of three or more muon hits. The muon times associated with the cluster are shifted in time by the displacement of the cluster center from zero. In 26% of the events no cluster is found and the times of these muons remain unmodified. Also shown in Fig. 26 is the muon time distribution after the cluster correction. The improvement is evident.

Once the timing of the muon hits is corrected for shower reconstruction and clustering, a narrow time window is chosen for selecting muon hits that are associated with the shower. Hits that arrive within the timing window are called "in-time" muons, while hits arriving outside the window are considered to be accidentals. The width of the timing window is chosen to include at least 95% of real shower muons. The size of the window is determined on a run by run basis. We find that the width of the timing window varies with the distance of the muon counter from the core of the shower. Typically it varies from about 35 ns for muon counters within 50 m from the shower core, to about 120 ns at 300 m from the core. The width of the timing window is independent of the number of muons in the cluster.

Fig. 27 shows the distribution of the number of in-time muons. About 5% of the showers (all small) have no muons at all. In Fig. 28 we plot the distribution of muons for large showers with ≥ 250 alerted stations. Of the 7.8×10^4 showers represented all but 100 have ≥ 30 muons. These 100 events represent for the most part a residual of events where an accidental trigger stops the muon TDCs before the large shower and the muons strike the array. Recently we have installed modified trigger electronics which will record for each event the arrival times of the first five trigger request pulses. In the reconstruction of the shower, the predicted trigger request arrival times must be consistent with those recorded. In this manner we can suppress events where the trigger requests include an accidental alert. We expect, then, a significant improvement in the hadron rejection for large showers.

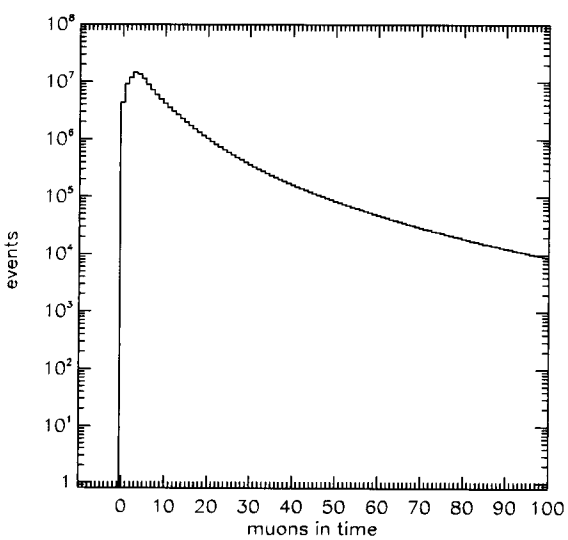

Fig. 27. Distribution of the number of muons-in-time for all events.

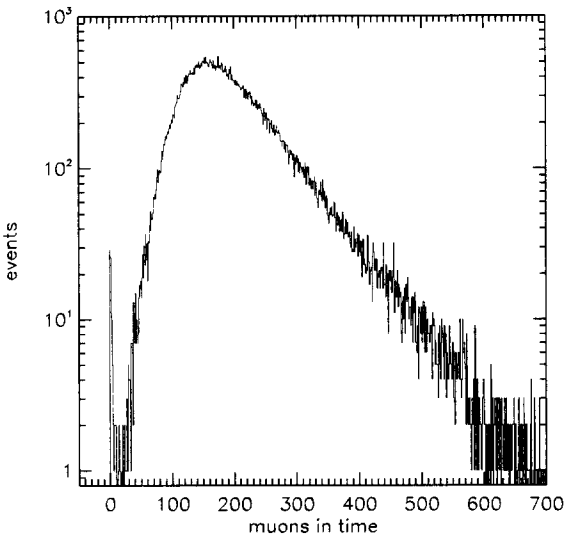

Fig. 28. Distribution of number of muons-in-time for showers with ≥ 250 alerts.

To characterize the muon content of individual events, we determine the expected number of muons, based upon the assumption that the overwhelming majority of real cosmic ray showers are hadronic, and then we select events which contain relatively few in-time muons hits. In considering the conditions for selecting such "muon-poor" showers, we must consider both the mean and the statistical fluctuations in the number of expected in-time muons. Since larger showers will have more in-time muons, we wish to scale the number of expected muons with a parameter that scales with the shower size, such as the number of alerted CASA stations. Fig. 29 shows the mean number of in-time muons versus the number of alerts. The correlation of these two quantities is evident. We also consider the dependence on the zenith angle and core location of the shower. Then, on a shower-by-shower basis, we can specify the muon content in terms of the

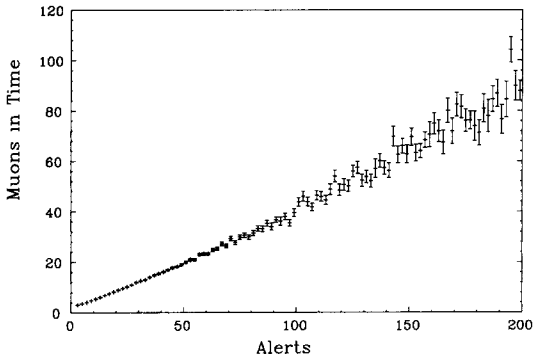

Fig. 29. Mean number of muons-in-time as a function of the number of alerted stations.

log ratio of the observed to expected in-time hits. We define the relative muon content r_μ as:

$$r_\mu \equiv \log_{10} \frac{(n_{\mu\text{-obs}})}{(n_{\mu\text{-exp}})},$$

where $n_{\mu\text{-obs}}$ is the number of in-time muons actually detected and $n_{\mu\text{-exp}}$ is the number of in-time muons predicted for hadrons. Fig. 30 shows the distribution of r_μ for a collection of real events. When a shower contains zero muons, as many of the smallest showers do, the shower is defined as muon-poor and is assigned a value of $r_\mu = -4.0$. Also shown in Fig. 30 is a distribution of the values of r_μ for a simulated set of γ-ray events generated with the MOCCA simulation. As can be seen in the figure, the distribution for γ-rays is shifted to the left of the normal cosmic ray distribution and contain a much larger proportion of zero-muon events.

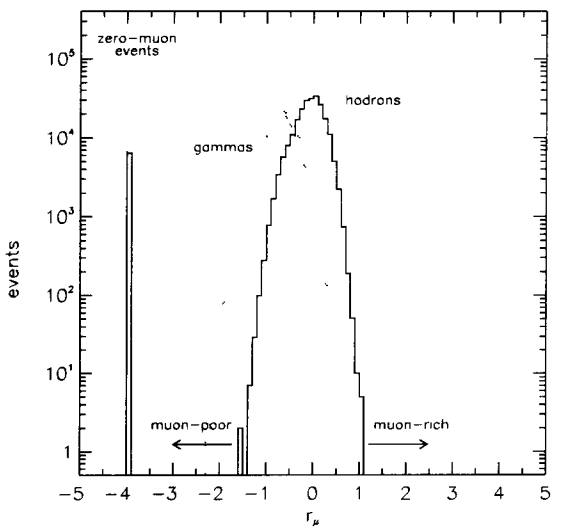

Fig. 30. Plot of r_μ for the data (solid histogram). The dashed histogram is the distribution expected for γ-rays based on the MOCCA simulation.

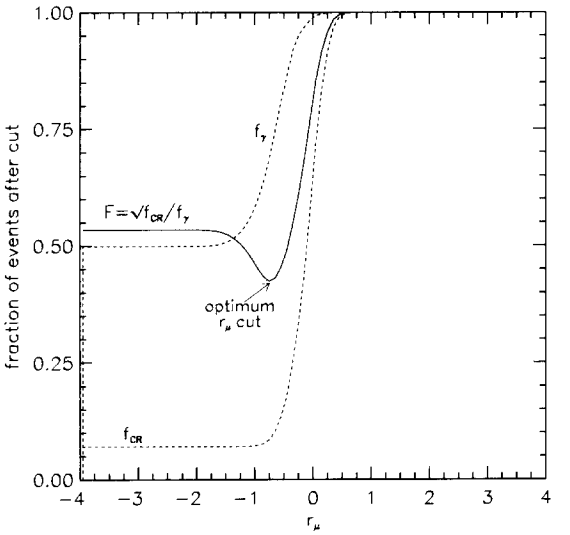

Fig. 31. Figure of merit as a function of the muon-poor cut in r_μ. Dashed lines show the fraction γ-rays and cosmic rays retained by the r_μ cut.

To reject hadronic background and thereby enrich the γ-rays in the sample, we cut events above some value of r_μ in our search sample. The optimum value of r_μ for the cut is determined by the minimum of the ratio: $F = \sqrt{f_{CR}}/f_\gamma$, where f_{CR} and f_γ are the fractions of normal (hadronic) cosmic ray and γ-ray showers retained after the cut. Fig. 31 shows a plot of these quantities as calculated for a set of real events. The ratio F represents the figure of merit for hadronic rejection based on the muon content. If a real γ-ray signal is observed its significance would be proportional to $1/F$. As indicated above, hadron rejection improves dramatically for larger showers. Fig. 32 shows the figure of merit for muon content cuts applied to samples of successively larger showers. For events with more than thirty CASA stations alerted, the sensitivity improvement achieved by the muon system is more than a factor of 10 compared to a system with no hadron rejection ($F = 1$).

A more classical method of rejecting hadron showers gives results similar to the one described above. In this method we use a maximum likelihood technique to compute the total shower size N_e in CASA and the total muon size (N_μ) in MIA. N_e includes both electrons and muons that impinge on CASA while N_μ is virtually pure muons that are recorded by MIA. The likelihood fit uses the appropriate NKG function [22] for the electron lateral distribution and the Greisen function [23] for the muon lateral distribution. The fits take proper account of the shower location and angle

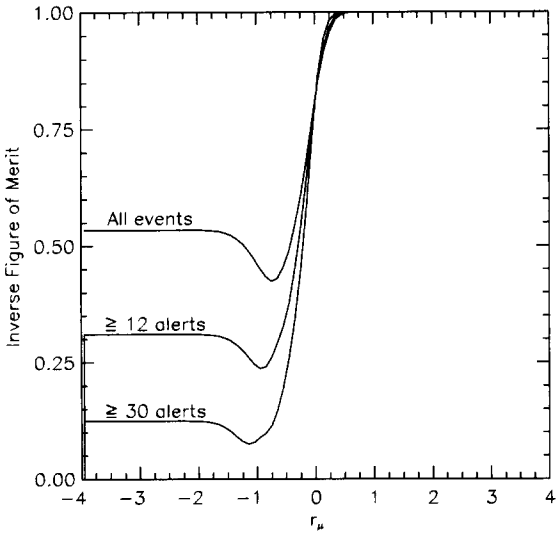

Fig. 32. Figure of merit for the muon-poor cut parameterized according to alerts.

as well as the counter efficiencies, alert requirements, and accidental alerts. The mean $\log(N_\mu)$ is parameterized for each run as a function of $\log(N_e)$ and zenith angle. The rejection variable (R_μ) for a given shower is then defined as:

$$R_\mu = \log(N_\mu) - \langle \log(N_\mu) \rangle .$$

The figures-of-merit of this method are similar to those shown in Fig. 32 and have minima near $R_\mu = -1$.

5. Operating experience with CASA-MIA

The first operation of CASA began on January 1, 1989 with a 49 station prototype array. At this time MIA consisted of the eight inner patches indicated in Fig. 1. This array ran until October 1989 with a trigger rate of 1.2 Hz. About 24 million events were collected and the results of this period have been published [24]. In February 1990 an enlarged array of 529 detectors began to operate. The trigger rate began at about 9 Hz and gradually increased to 12 Hz as various faults in the trigger system were removed. Data were collected with 529 detectors while the remainder of CASA and the 8 outer patches of MIA were installed. About 280 million events were accumulated through December 1990 and results of an all sky survey were published [25].

In late March 1991 the full array of 1089 stations began operation with a rate of 22 Hz. On April 22, 1991 the array was struck by lightning and severely damaged. It did not resume operation until January 1992. On the advice of a consultant [26] lightning protection was installed. The entire array has been enclosed in a very coarse Faraday cage consisting of wires spaced ~30 m apart suspended by grounded poles 4 m above the array. A similar mesh was placed on the ground attached to the poles supporting the overhead wires. Also spark gaps and MOVs (metal oxide varisters) have been installed at appropriate places on the AC power distribution and the trigger request, trigger acknowledge, and Ethernet cables. In addition, the central station has been electrically isolated from the dual Ethernet spines using fiber optics.

Fig. 33 shows the total accumulated triggers as a function of time collected through November 1993. Due to various malfunctions, shutdowns, power failures, and quality cuts on the data, the ratio of live-time to actual time is about 92%.

5.1. Instrument maintenance program

Normally CASA-MIA can be run by a single operator. The only activity that strictly requires daily operator action is the changing of 8 mm data tapes. The remaining operator effort is directed towards maintenance of the array, particularly repairs to occasionally failing components within the 1089 stations. During the prototype and installation stages of the experiment, maintenance efforts were fairly high, with several new component failures occurring each day. Typically, these "low-level" component failures affected the operation of some 5% of the operating stations within the array.

One of the most common components to fail are the LT1016 comparators. Before the installation of the Faraday cage even distant lightning could damage the LT1016s. Counters can also fail; the glue joint of the PMT to the scintillator can break or the base of the PMT can develop an arc. On a few occasions cables have been chewed by burrowing animals.

In 1992, a systematic maintenance program was developed to correct all remaining instrument prob-

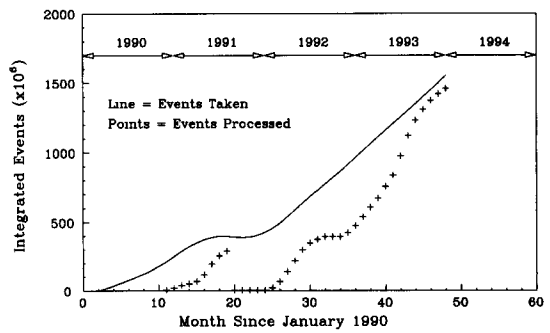

Fig. 33. Accumulated triggers of CASA-MIA as a function of time. Also shown is the accumulated number of events processed.

lems in the array. The goal of the program was to optimize sensitivity and to reduce the level of daily maintenance required. The program combined several initial intensive repair efforts with detailed tracking of component failures in the array. Three major array component systems were addressed: electronics boards, scintillation counters, and power supplies and connectors.

5.2. Repairs to station electronics boards

During the summer of 1992, as many as 5% of the 1089 stations contained boards with some sort of electronics problems. Most of these problems fell into two broad categories:

Some boxes failed intermittently such that they did not collect data or else did not transmit collected data to the central processor. By tracking the performance of all stations over several weeks of time, all such malfunctioning boards were identified and replaced or repaired. Fig. 34 shows the average percentage of all stations transmitting data. By the end of 1992, more than 99.8% of all stations were transmitting data. Typically there are less than three such malfunctioning stations in the array. The current failure rate for this problem is very low; typically one new failure occurs every week or two.

Many stations retained minor analog circuitry problems which affected timing and pulse height information from individual channels. Boards with these problems were systematically identified and repaired. The failure rate for new analog board problems remains low, with one new failure occurring every few days.

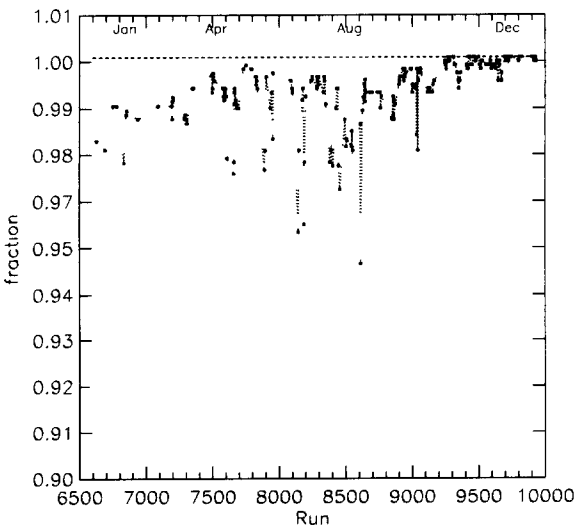

Fig. 34. The average fraction of CASA stations collecting and reporting data during runs obtained in 1992.

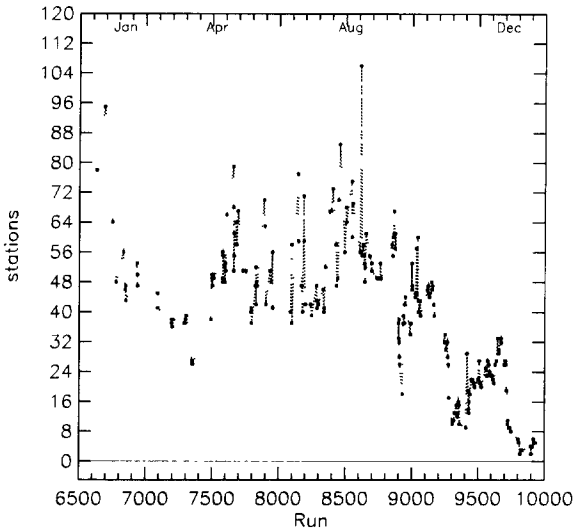

Fig. 35. The number of stations in the array with malfunctioning scintillation counters in 1992.

5.3. Repairs to scintillation counters

During the Fall of 1992, a program was initiated to track the detailed performance of each of the 4356 scintillation counters located within the surface array stations. Over two hundred problem counters were identified and repaired in the field or replaced. Some of the most common problems discovered were:

Water damage to PMT base circuitry and components: Many of the damaged bases were successfully cleaned and repaired. This damage occurred prior to the installation of the covers as mentioned in section 2.2.1.

Failure of optical cement to bond PMT to scintillator: These counters were cleaned and re-glued.

Counter light leaks: Small holes and tears were located and closed.

Failed phototubes: Several dozen phototubes demonstrated significant degradation in output gain. These counters were replaced.

Fig. 35 shows the average number of problem counters in the array during 1992. As a result of these counter repair efforts, the number of problem counters in the array has been reduced to negligible levels. Currently the failure rate for counters is low; typically one new counter problem occurs every week.

Additionally, a program was begun to systematically balance counter gains within each station, and from station to station, so as to obtain an optimally uniform gain response over the entire array. To accomplish this, counters were rearranged within nearly 200 imbalanced stations and an automated program was developed to fine tune high-voltage levels for each station.

5.4. Repairs to power supplies and connectors

Each surface station contains a low-voltage DC power supply and a high-voltage DC–DC converter. In the first six months of 1992, as many as 50 of each of these supplies failed. Most of the low-voltage supply failures probably resulted from moisture in the boxes. Additionally, the connectors between the low-voltage supplies and the boards in dozens of stations were found to be slightly corroded. This corrosion degraded the +5 V power input to the boards such that these boards would malfunction.

To address these problems, all damaged power supplies were repaired or replaced, and all corroded connectors were cleaned and lubricated. Since the installation of the weatherproof covers, moisture damage and corrosion have been dramatically reduced. Presently, the failure rate for power supplies and connectors is low; typically one new failure occurs every week.

5.5. Results of maintenance program

The basis of the maintenance program implemented in Fall of 1992 was a systematic procedure for tracking instrumental problems combined with several intensive repair efforts to repair specific components of the array. One result of this program has been a steady improvement in the average trigger rate, which scales directly as the sensitivity of the experiment. Fig. 36 is a plot of the trigger rate during 1992, which shows an overall increase as a result of the maintenance and repair program.

Additionally, since the completion of the 1992 program, the daily maintenance required to address new instrumental problems has been substantially reduced. Thus, we anticipate continued experiment operation at fully optimum performance levels with minimal future maintenance efforts.

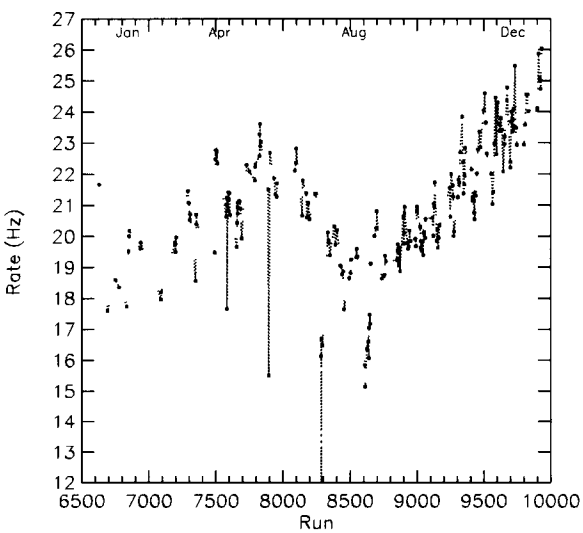

Fig. 36. The trigger rate of the array for 1992.

5.6. Longterm muon counter stability

The components of MIA must be robust since their burial precludes maintenance. The design goal was a counter lifetime > ten years. We have been encouraged by the success of the water-tight PMT enclosures and the passive electronics components in the bases. Only 41 of the 1024 counters have terminally failed after burial times ranging from two to six years. Over half of these ceased operation shortly after installation. Since early 1991 (the completion date of the full 16 patch system) the unrecoverable failure rate has been < 0.4% per year.

The majority of the routine counter failures occur in the above-ground discriminator and signal-repeater electronics and are easily diagnosed and repaired. More rarely, failures occur in the cable connections in outdoor junction boxes which are placed about every 60 m between a patch and the central station. These are almost always due to deterioration of solder connections from water condensation or seepage.

Acknowledgements

The construction of CASA-MIA involved the effort of many individuals. In the development of the design concept for CASA-MIA, discussions with George Cassiday of the University of Utah were stimulating. In the design of the electronics we acknowledge the contributions of Michael Pertel (deceased) of the Laboratory of Astrophysics and Space Research (LASR) of the University of Chicago. Joe Ting of the University of Chicago Electronics Development group was responsible for a number of the analog circuit designs. The mechanical design of the prototype array was greatly assisted by Wayne Johnson of LASR. Mechanical design of the full array was carried out by Elizabeth Pod and Richard Armstrong of the University of Chicago Engineering services group. Thanks go to many undergraduate students who labored to build and to install the CASA detectors. Leon Mualem, Joe Reese, John Loeffler, Ann Parsons and Bob Render worked tirelessly on the installation of the MIA counters. John Mann played an essential role in the development of the MIA electronics. We especially acknowledge the University of Chicago students who wrote senior theses on a number of subjects related to CASA while working on the project. These are Adrian Cho, Ashraf el-Far, Karl Christensen, Paul Haar, John Kim, Peter Burke, and Sunil Golwala. The assistance of Ron

Cooper of the University of Utah in making arrangements with the US Army at Dugway was crucial to the success of the project. We acknowledge the encouragement and assistance of the Cosmic Ray group at the University of Utah: Steve Corbato, Jerry Elbert, Dave Kieda, Eugene Loh and Pierre Sokolsky. We acknowledge the active participation of Mark Wiedenbeck (LASR) in the early stages of the project. The cooperation of the command and staff of the US Army Dugway Proving Grounds was essential for the success of this project. Finally we acknowledge the support of the U.S. Department of Energy and the U.S. National Science Foundation for the financial support that made this project possible.

References

[1] G. Cocconi, Proc. 6th Int. Cosmic Ray Conf., Moscow, 2 (1960) 309.
[2] M. Samorski and W. Stamm, Ap. J. 268 (1983) L17.
[3] J. Lloyd-Evans et al., Nature 305 (1983) 784.
[4] T. Kifune et al., Ap. J. 301 (1986) 230.
[5] D.E. Alexandreas et al., Nucl. Instr. and Meth. A 331 (1992) 350;
A.X. Huo et al., Proc. 21st Int. Cosmic Ray Conf., Adelaide, 2 (1990) 427;
F. Aharonian et al., Proc. 22nd Int. Cosmic Ray Conf., Dublin, 4 (1991) 452.
[6] D. Ciampa et al., Phys. Rev. D. 46 (1992) 3248.
[7] A.A. Watson, 19th Int. Cosmic Ray Conf., La Jolla, 9 (1985) 111;
R.J. Protheroe, 20th Int. Cosmic Ray Conf., Moscow, 8 (1987) 21;
D.J. Fegan, 21st Int. Cosmic Ray Conf., Adelaide, 11 (1990) 23;
J.W. Cronin, K.G. Gibbs and T.C. Weekes, Ann. Rev. Nucl. Part. Sci. 43 (1993) 883;
D.E. Nagle, T.K. Gaisser and R.J Protheroe, Ann. Rev. Nucl. Part. Sci. 38 (1988) 609.
[8] K.G. Gibbs, Nucl. Instr. and Meth. A 264 (1988) 67;
R.A. Ong, Nucl. Phys. B (Proc. Suppl.) 14A (1990) 273.
[9] D. Sinclair, Nucl. Instr. and Meth. A 278 (1989) 583.
[10] R.M. Baltrusaitis et al., Nucl. Instr. and Meth. A 240 (1985) 410.
[11] The scintillator was manufactured by the Polycast Technology Corp., Stamford, Conn.
[12] The silicone used was the two component RTV, GE-655. Before gluing, the surface of the PMT and the plastic were treated with the primer GE 4120. These materials are manufactured by the General Electric Co.
[13] These supplies were manufactured by Condor Electric, Oxnard, CA.
[14] The DC to DC converters were manufactured by the EMCO Corp., Sutter Creek, CA.
[15] A 0.1-in. terminal post connector (model AMPMODU) manufactured by Amp Inc., Harrisburg, PA.
[16] T.F. Droege and T. Ohska, IEEE Trans. Nucl. Sci. NS-29 (1982) 299.
[17] Repeaters manufactured by Garrett Communications, San Jose, CA.
[18] J. Elbert et al., 22nd ICRC, Dublin 1 (1991) 281.
[19] A. Borione et al., Phys. Rev. D 49 (1994) 1171.
[20] A.M. Hillas, University of Leeds, Private communication. We gratefully acknowledge the permission to use the shower simulation program MOCCA. All simulations referred to in this paper use the MOCCA program.
[21] T. Stanev, T.K. Gaisser and F. Halzen, Phys. Rev. D 32 (1985) 1244;
T.K. Gaisser et al., Phys. Rev. D 43 (1991) 314.
[22] K. Kamata and J. Nishimura, Prog. Theor. Phys. (Kyoto) Suppl. 6 (1958) 93;
K. Greisen, Prog. Cosmic Ray Phys. 3 (1956) 1.
[23] K. Greisen, Ann. Rev. Nucl. Sci. 10 (1960) 63.
[24] J.W. Cronin et al., Phys. Rev. D 45 (1992) 4385.
[25] T.A. McKay et al., Astrophys. J. 417 (1993) 742.
[26] P. Kreider, Univ. of Arizona, private communication.